CONTENTS

SCIENTIFIC AND TECHNICAL

INDUSTRIAL

INCREASE IN THE LIFE OF WELDED JOINTS OF AMg6 ALUMINUM ALLOY

L.M. Lobanov, M.O. Pashchyn, O.M. Tymoshenko, P.V. Goncharov, O.L. Mikhodui and **K.V. Shiyan**

E.O. Paton Electric Welding Institute of the NAS of Ukraine
11 Kazymyr Malevych Str., 03150, Kyiv, Ukraine. E-mail: office@paton.kiev.ua

The effect of electrodynamic action on the life of welded joints of AMg6 aluminum alloy under cyclic loading was investigated. It was found that electrodynamic treatment of specimens of butt welded joints of AMg6 alloy results in reducing the level of residual tensile welding stresses, which is followed by their transition to compression. It is shown that as a result of double-sided single-channel electrodynamic surface treatment in welded joints of AMg6 alloy, the cyclic life is three times increased as compared to the initial one. Additional electrodynamic treatment of the fusion line five times increases the life as compared to the non-treated metal. In the comparative evaluation of single- and two-channel electrodynamic treatment of specimens, it was found that the increase in life when using a two-channel scheme (as compared to single-channel) is determined by the controlled synchronization of components of electrodynamic effect, which eliminates the passage of electric current pulse through its treated metal in the phase of its attenuation. It was shown that at electric pulsed action, the life of two-channel treated specimens is more than 50 % higher than that of the dynamic ones, which is connected with the contribution of electroplastic effect to the reduction of residual welding stresses. 8 Ref., 4 Tables, 5 Figures.

K e y w o r d s : electrodynamic treatment, electrode device, single- and two-channel scheme, residual welding stresses, aluminum alloys, life, electric current pulse, cycle amplitude

The use of modern ship hull and transport welded structures of aluminum-based alloys requires new approaches to increase their life. The solution to the problem of inhibiting the development of fatigue fracture is relevant for the life extention of both the new and existing machines [1].

To increase the fatigue resistance of structural materials, a number of effective ways is available based on the induction of compressive stress fields in the area of predicted fracture, among which high-frequency mechanical peening can be mentioned [2]. The methods of increasing fatigue based on reducing the stress concentration include treatment of the crack tip with pulsed electromagnetic fields of different duration and configuration [3].

One of the methods of electropulsed effects on welded joints is electrodynamic treatment (EDT) [4], the results of which are a decrease in the level of residual welding tensile stresses, which is accompanied by the formation of a layer of metal with refined structure in the treatment zone. The analysis of the results [1–4] gives grounds to suppose that EDT can be an effective way to increase the life of welded joints. At present, there are no data regarding evaluation of EDT effect on the life of welded joints.

The aim of the work was to study the effect of electrodynamic actions on the life of welded joints of aluminum AMg6 alloy under cyclic loading.

EDT of the welded joint was performed using single-channel and two-channel circuits of the electrode device (ED).

Single-channel electrode device. *Design scheme of single-channel ED.* The design scheme and appearance of a single-channel ED are presented accordingly in Figure 1. ED provides an electric contact between the discharge circuit and the metal treated in one channel, through which a pulse of electric current — EPC is introduced to the latter. ED provides the ability to regulate the dynamic and electropulse effects of the electrode on the metal. The working body of ED is the electrode *1* (Figure 1, *a*), which is fixed in the brass casing *2* with a screw *3*. The working surface of the electrode, which contacts with the metal *22*, is polished and has a radius of curvature being *15* mm. The casing *2*, rigidly connected to the copper *8* and steel (stainless steel) *7* disks with a thickness of 3 and 5 mm together with the electrode *1* form a part of the impact mechanism (IM).

IM is fixed in two teflon sliding bearings *11*, which allow them to move in the vertical direction. The rotation of the IM around its own vertical axis is prevented by two screws *4*, which move in the vertical grooves of the ring *5*.

The disks are connected to the housing *12*, in which the inductor *10* is located, which is wound with the copper bus 6.2×1.5 mm and has 18 turns. Due to the ge-

L.M. Lobanov — http://orcid.org/0000-0001-9296-2335, M.O. Pashchyn — http://orcid.org/0000-0002-2201-5137,
O.M. Tymoshenko — https://orcid.org/0000-0001-9163-1067, P.V. Goncharov — https://orcid.org/0000-0002-1980-2340,
O.L. Mikhodui — http://orcid.org/0000-0001-6660-7540, K.V. Shiyan — https://orcid.org/0000-0001-9198-6554
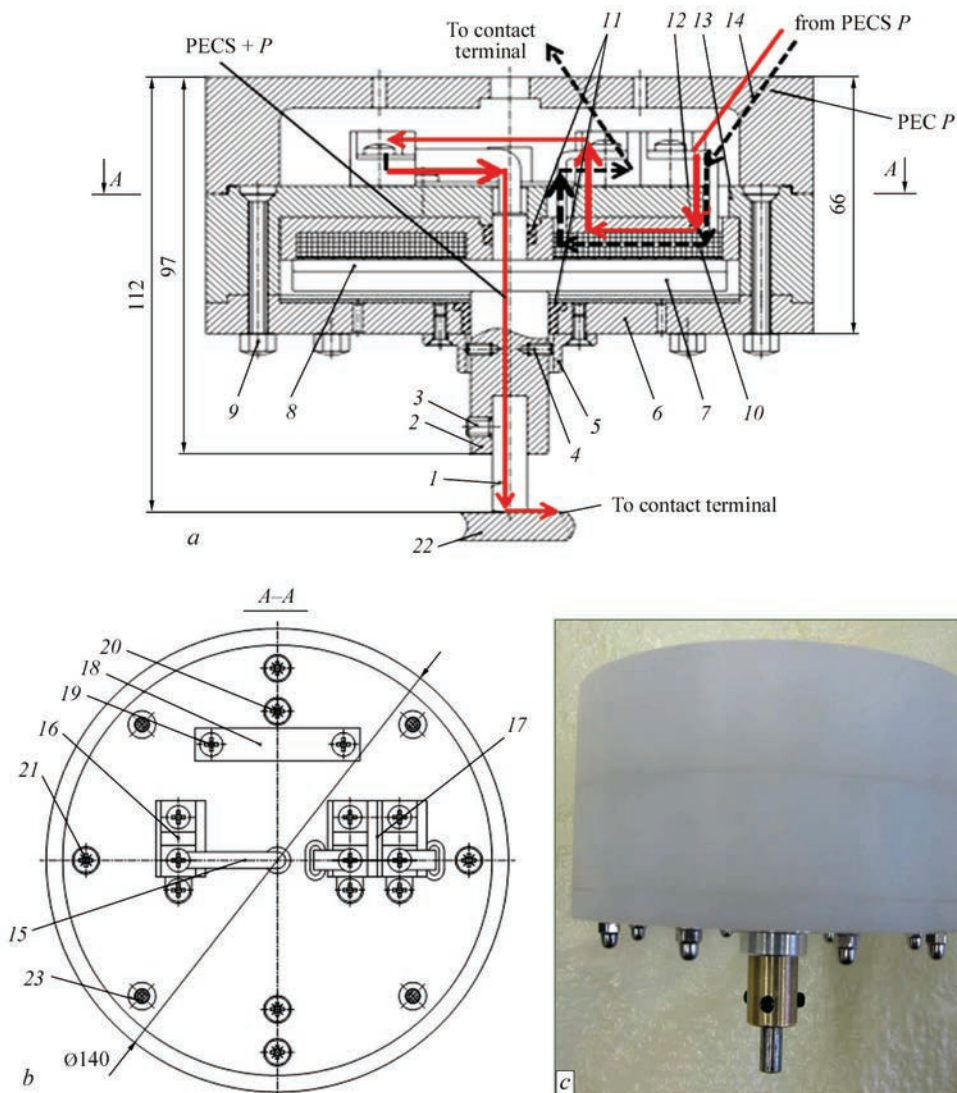
Fig re 1 Design scheme of single-channel electrode device (ED) for EDT (see explanation in the text): *a* — side view, arrows show the direction of PEC; *b* — top view; *c* — single-channel ED for EDT

ometry of the housing, between the copper disk and the winding a nonmagnetic gap of 0.5 mm is maintained. The inductance of the coil is 14.66 μH. The housing *12* is fixed on the base *13* by screws *20*. From the bottom to the base *13* by screws *21* and nuts *9* the lower cover *6* is attached, on the inner surface of which, a rubber gasket is located, designed to dampen the electrodynamic impact on the lower cover when the electrode does not rest on metal. To connect the ED to the pulsed current source on top of the base *13*, the terminals *16* and *17* are located (Figure 1, *b*). By means of the terminal *16*, the supply of pulsed electric current (PEC) 1 to the impact mechanism through the flexible wire *15* and by the terminal *17* the winding switching are performed.

Single-channel ED has two variants of switching:

1) realization of interaction of electropulsed *I* and dynamic *P* effects — PEC *I* + *P*;

2) effect of only the dynamic load *P* — PEC *P* (Figure 1, *a*).

Principle of operation of single-channel ED. During the interaction of *I* and *P* to one of the ends

of the winding of the terminal *17*, the positive wire is connected from the pulsed electric current source, the other ends of the winding is connected to the impact mechanism by the terminal *16*, and the negative wire from the pulsed electric current source (PECS) is connected to the treated metal *22*. The scheme of PEC *I* + *P* flow is shown by a solid arrow in Figure 1, *a*. Under the dynamic effect, the wire from the PECS is connected to the two ends of the terminal *17*, and terminal *16* is not connected. In this case, PEC *P* flows in the direction indicated by the dotted arrow in Figure 1, *a*. The wires are fixed with a clamp *18*, which is attached to the base *13* by means of screws *19*. From the top the terminal department is closed by the cover *14* which is attached to the base by screws *20*, *23* and nuts *9*.

ED operates as follows. ED rests on the metal with the end of the electrode and is exposed flatwise to the treatment surface. For normal operation of ED in order to prevent sparking and melting at the place of the contact «electrode–metal» before the supply of PEC,

Fig re 2 Oscillograms of dynamic pressure *P* and pulsed current *I* passing through the treated metal on one-channel (*a*) and two-channel (*b*) schemes of ED

it is necessary to provide a guaranteed pressing of the electrode to the treatment surface.

At the correct positioning of ED, through the impact mechanism the load force is transmitted from the housing to the tungsten electrode and leads to p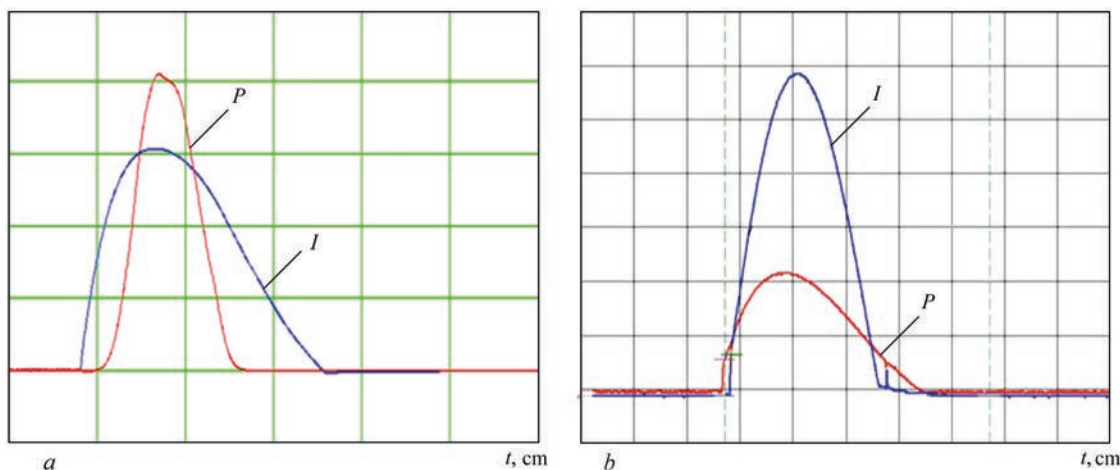ressing of the electrode to the metal surface. When PEC flows through the induction coil *10* in the disk *8*, the eddy currents are induced, at first providing the repulsion of the disk from the coil, and then at the end of the pulse — attraction to it.

Advantages of single-channel ED. The design of the single-channel ED, based on the scheme of direct passing of PEC, has a number of advantages, which include the ease of manufacturing the device and minimal energy losses in it during operation of the pulsed current source in the discharge cycle. The ED design with direct passing of PEC through the inductor and the electrode is featured by a shorter duration of the dynamic load pulse *P* as compared to PEC — *I* (Figure 2, *a*), as well as the lack of possibilities for a controlled synchronization of the electropulse and dynamic effects. This narrows the possibilities of controlling the EDT process, but everything is compensated by the simplicity of manufacturing and operation of ED.

From the standpoint of electrodynamics, ED with a treated welded joint, which is included in the discharge circuit with the power source, is represented in the form of magnetically coupled circuits, in the primary circuit of one of which a capacitive energy storage is included.

Two-channel electrode device. In order to eliminate the disadvantage inherent in magnetically coupled circuits, a two-channel ED based on magnetically decoupled circuits was developed and manufactured, which includes two independent channels of PEC *I* and PEC *P*. The first channel forms PEC *P* (Figure 2, *b*), which is designed to create a dynamic pressure on the treatment zone and is supplied to the induction coil of ED. The second channel forms PEC *I* (Figure 2, *b*), consistent in duration with the period of dynamic pressure on the treatment area. PEC *I* is supplied directly to

the electrode of ED and can be transferred to the treated switching. At the same time the scheme of ED allows switching off the second channel (PEC *I*) and transferring only dynamic pressure to a product. The electric circuit of the second channel is closed through a contact cable, which is attached to the product.

Design scheme of two-channel ED. As to its design, the two-channel ED (Figure 3, *a*) consists of the electrode *1* fixed in the housing *3* by the fixation devices *2* and *20*. The housing is connected with the disk of nonferromagnetic material *16*, which rests on the frame *6* with the inductance coil *14* placed in it with a built-in flat inductor *15*. The coil is fixed to the frame by screws *11*. The lower wall of the frame *4*, fixed by screws *5*, acts as a nonmagnetic substrate under the disk and the damper *17*. The upper (protective) cover *9* of the frame is fixed in the body of ED by screws *8*. The supply of PEC *I* to the coil is performed by the wire *7*. The short circuit of the discharge circuit, providing the supply of PEC *I* to the workpeace *18* is carried out by the terminal *19*. PEC *P* passes through the coil on the wires *12*, *13*. The supplies *7*, *12*, *13* of ED are connected to external circuits by the contact terminals *10*.

Principle of operation of two-channel ED. Two-channel ED during EDT operates as follows. When a pulsed current flows through the coil, a magnetic field is excited, which initiates eddy currents in the disk. The interaction of the induced currents with the magnetic field, by which they were initiated, leads to the generation of electrodynamic force. In the first phase of the effect, the electrodynamic force presses the electrode to the treated material, and in the second direction the force changes to the opposite one — the electrode is repelled from the treated material. The effect of the pulsed current on the treatment zone does not exceed the duration of the pressing force in terms of duration (see Figure 2, *b*). The design of ED is subjected to the requirements of the consistent pulse duration and the exclusion of electrospark phenomena in the treatment zone. The control of channels in
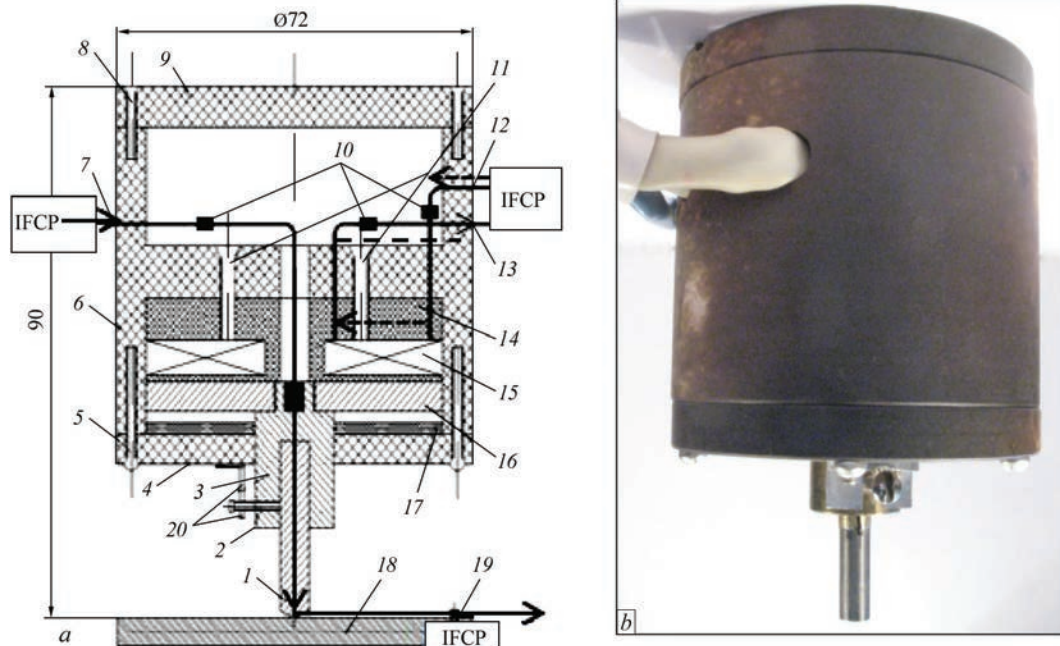
Figure 3 Two-channel electrode device (ED) for EDT with independent PEC channels: *a* — design scheme, where the arrows show the directions of PEC *I* and PEC *P* (see explanation in the text); *b* — appearance of ED

ED is performed in three microcontrollers and on a programmable logics, which allows controlling the parameters of current pulses (amplitude), the delay of a one pulse relative to another, as well as visualizing the parameters of pulses on the light display. The duration of pulses on both channels is determined by the parameters of the electric circuit of the discharge circuits and can be changed discretely by increasing/decreasing their inductance.

Advantages of two-channel ED. To provide the normal mode of operation of ED, which eliminates sparking and melting at the point of contact «electrode-specimen», the value of static load was determined, which provides a reliable current contact of the electrode with the treated surface. For this purpose, a guaranteed static pressing of the electrode *1* of ED (Figure 1, *a*) was created to the outer surface of the specimen *22*, for which the welded joint was used shown in Figure 4. On the pressing force F_y the R_c value of the electrical resistance of the contact «electrode-specimen» significantly depends. To evaluate the effect of F_y on changes of R_c, R_c values were measured by varying F_y in the range from 2 to 150 N. For this purpose, on the outer surface of the cover *14* of ED (see Figure 1, *a*), the loads of different mass were mounted and the changes in R_c values were recorded on the area of the discharge circuit between the electrode *1* and the specimen *22* with the use of the measuring bridge (LC-meter) of BR2876-5 grade. Dependence of the contact resistance R_c on the force F_y of static pressing of the electrode to the specimen is presented in Table 1, from which it is seen that with increase of F_y from 2 to 40 N, the value of the resistance R_c decreases intensively from 90 to 13 mOhm.

At a further increase in F_y to 150 N, R_c decreases linearly to 10 mOhm. From the data in Table 1 it can be concluded that an increase in F_y to more than 40 N has a negligible effect on the change in resistance in the zone of contact interaction. This determined the choice of F_y value in the subsequent experiments, which was in the range of 50–80 N.

Investigation of EDT effect on fatigue resistance of specimens of welded joints of AMg6 alloy. The specimens with a thickness $\delta = 2$ mm (Figure 5) were produced by automatic TIG (Ar) welding at an arc volt-
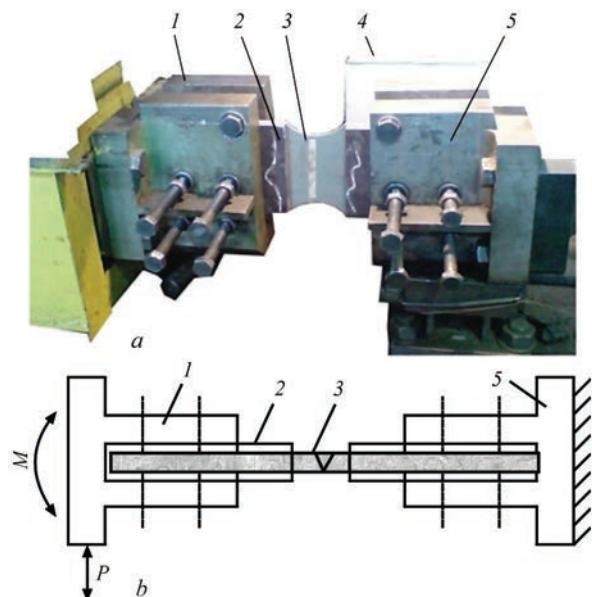

Figure 4 Fatigue tests of specimens of welded joints of AMg6 alloy after EDT: *a* — appearance of UPM-02 testing machine (*1* — movable clamp; *2* — fixing plate; *3* — specimen; *4* — cycle counter; *5* — fixed clamp); *6* — scheme of tests; *P* — horizontal load; *M* — bending moment

5

Table 1 Dependence of resistance of contact R_c on the force of static pressing of the electrode to the specimen F_y

F_y, N	2	3	10	15	22	40	80	150
R_c, mOhm	90	40	25	20	15	13	12	10

age $U_w = 20$ V, welding current $I_w = 170$ A and welding speed $v_w = 5.5$ mm/s. By using the method of electronic speckle interferometry [5], the values of residual welding stresses in the central elongated cross-section of the specimen were determined corresponding to the line $A–A$ in Figure 5 before and after EDT. EDT was performed in the direction «from the center to the edges» (arrow in Figure 5), using an electrode device (ED), equipped with a tungsten electrode of VL grade with a hemispherical working end, and the EDT mode provided a stored energy of the capacitor E_s up to 600 J at a single electrodynamic effect.

The treatment of specimens was performed by the electrode device in the conditions of «rigid fixation», for realization of which before EDT both sides of the specimen (Figure 5) were «rigidly» fixed by a distributed load on the assembly plate, excluding the probable angular deformations of the specimen. Such a scheme of fixation of the treated metal, on [6], provides the maximum efficiency of electrodynamic effect at other equal parameters of the EDT mode. The treatment was performed at the value of ED inductance $L = 5.3$ µH and the energy $E_s < 1$ kJ. When choosing the values of the charging voltage U for two EDT schemes, the researchers were based on the fact that the values of $U_I + U_P$ for a single-channel scheme and the total $U_I + U_P$ for a two-channel scheme should be equal. Thus, in a single-channel scheme the EDT mode was used, which is set as follows $U_{I+P} = 570$ V ($I = 5.75$ kA) for PEC $I + P$, and in a two-channel scheme $U_P = 200$ V ($I_p = 1.45$ kA) for PEC P and $U_I = 370$ V ($I_I = 4.3$ kA) for PEC I.

To realize the electrodynamic effect on the working part of the specimen in the EDT zone, ED was installed and its guaranteed electrical contact with the treated surface was provided when the discharge circuit was closed. The switching of the power key initiated the discharge of the capacitive energy storage through ED into the treated material. In the process of performing EDT with a series of PEC, ED was moved along the surface of the treated area of specimens in the direction «from the center to the edges» (arrow in Figure 5) with a step of 3–5 mm. In each EDT cycle, up to 35 electrodynamic effects were performed, which provided a uniform surface electroplastic deformation of the treated weld area (fusion line) with a length of 90 mm. On one- (Figure 1) and two-channel (Figure 3) schemes of EDT, different schemes of specimens treatment were realized, which were performed from the outer surface of the weld and the fusion line, as well as from the root side of the weld.

The fatigue tests of the specimens were performed, which were treated on different EDT schemes. The machine of the grade UPM-02 was used (Figure 4), which realizes the scheme of fatigue bending tests (Figure 4, *b*) at a symmetrical load cycle with a frequency of 14 Hz. The amplitude of the loading cycle σ_a was set in the range of 80–160 MPa, and the loading was carried out during the incubation period [7] until the number of cycles N was registered, corresponding to the beginning of the fracture of the specimens. The effect of different EDT schemes on the cyclic life N of specimens was investigated.

Analysis of the obtained results. The distribution of σ_x before and after the double-sided EDT of the weld center on the single-channel scheme is presented in Table 2. Table shows that before EDT the peak values of tensile stresses close to $\sigma_{0.2}$ for AMg6 alloy in the weld center and on the fusion line (in the zones of a probable fracture), after treatment were transformed into compressive stresses, the values of which reached -10 MPa.

The values of σ_y stresses in the center of the weld and on the fusion line before EDT on a single-channel scheme reached 12 and 17 MPa, respectively. After EDT, σ_y were transformed into compressive stresses, the values of which in the center of the weld and on the fusion line reached -68 and -56 MPa, respectively.

The features of schemes, location of the fracture zones and the value N are presented in Table 3. From its data it can be seen that as a result of double-sided EDT of the outer surface and the root of the weld on a single-channel scheme of ED, the cyclic life N of the specimens of welded joints in the studied range of σ_a is three times increased (lines 4, 7, 8) as compared to the original one (lines 1–3). The fracture of both the original specimens as well as those, which were treated, occurs along the fusion line. The data of Table 3 for a single-channel scheme confirm the results of fatigue tests, presented in Table 4.

The additional EDT of the base metal at a distance of 10 mm from the fusion line (line 5) provides a more developed zone of compressive stresses in the area of predicted fracture of specimens. Increase in the compression zone created in the vicinity of the welded
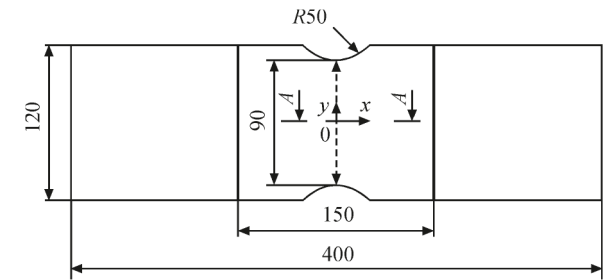

Figure 5 Scheme of specimens of welded joint of AMg6 alloy for fatigue tests, where the dashed arrow indicates the direction of EDT, $A–A$ is the cross-section, in which the stresses σ_x and σ_y were determined

Tb le 2 Distribution of σ_x before and after EDT (Figure 5) on a single-channel scheme

X, mm	0	5	11	16	25	36	46	56	66	76
σ_y before EDT, MPa	120	130	100	40	−40	−38	−28	−21	−18	−10
σ_y after EDT, MPa	−8	−9	−10	−10	5	18	15	11	2	−7

joint does not affect the life N. At the same time, a preliminary cyclic loading of the specimens before reaching $N_1 = 400000$ before EDT (line 6) leads to an increase in the life N. Comparing the data of lines 6 and 1 of Table 3, it can be seen that a preliminary cyclic stimulation of the specimens three times increases their life. This fact can be explained by the additional relaxation of residual welding stresses, which is provided by a preliminary cyclic loading of the specimens to the value N_1. Thus, the efficiency of EDT can be increased during the treatment of the welded joints, which are operated under cyclic loads, as compared to the manufactured ones.

The use of double-sided EDT using a two-channel scheme of ED has a positive effect on the life N, the value of which at $\sigma_a = 160$ MPa after a one- and double-sided EDT of the weld are increased by 6 and 15 %, respectively (lines 11 and 12 in Table 3) as compared to a single-channel one (line 8). The fracture zone is shifted to the base metal by 5–10 mm from the fusion line. The comparison of the lines 8 and 12 is interesting provided by the fact that the increase in N during the use of a two-channel scheme was achieved due to the realization of a twice lower number of effects than that used during a single-channel one (excluding EDT on the side of the weld root).

The additional EDT of the fusion line (line 13) increases the value of N twice as compared to a single-channel treatment of the weld alone (line 8) and

five times as compared to the original one (line 3). The increase in the N values during the use of a two-channel scheme can be explained by the peculiarities of a controlled synchronization of the components of an electrodynamic effect, which eliminates the passage of PEC through the treated metal in the phase of attracting the disk *16* to the coil *14* (Figure 3, *a*). This eliminates the thermal effect of PEC during the period of breaking the electric contact of the discharge circuit, which leads to the strengthening of the treated metal to a level higher than that of the base one. This results in shifting of the fracture zone from the fusion line into the base metal, which is shown in Table 3 (lines 9, 11).

The impact of the current component of the electrodynamic effect (PEC *I*) on the life N of welded joints during EDT on a two-channel scheme of ED was studied. For this purpose, the specimens were studied, that were treated under the conditions of interaction of electropulsed and dynamic effects (PEC *I* + PEC *P* — line 9), as well as only under dynamic effect (PEC *P* — line 10). From the Table 3 it follows that the value N under the conditions of interaction is more than 50 % higher than under dynamic loading. This fact can be explained by the contribution of the current component of EDT, which initiates the contribution of the electroplastic effect (EPE) [8] in reducing the level of residual welding stresses. The effect of stresses on the life N is especially significant at a multicyclic load, which corresponds to $2\sigma_a = 80$ MPa. The factor that determines the increase of

Tb le 3 Values of life N at different amplitude of cycle $2\sigma_a$ of welded joints of AMg6 alloy after EDT on one- and two-channel schemes of ED

Number of specimen series	EDT scheme	$2\sigma_a$, MPa	N	Fracture zone
1	Without EDT	80	525600	Along the fusion line
2	Same	120	210600	Same
3	»	160	151200	»
4	Single-channel, double-sided (weld + root)	80	1004800	»
5	Single-channel, double-sided (weld + root + BM on both sides at a distance of 10 mm from the fusion line)	80	970000	Base metal (BM) at 2 mm from the fusion line
6	Similarly to No.5, before EDT the specimen was loaded $N_1 = 400000$ at $\sigma_a = 80$ MPa	80	932000, taking into account N_1 — 1332000	Along the fusion line
7	Single-channel, double-sided	120	568000	Same
8	Same	160	360600	»
9	Two-channel: PEC *I* + PEC *P* (double-sided)	80	1169320	BM at 5 mm from the fusion line
10	Two-channel: PEC *P* (double-sided)	80	752400	Along the fusion line
11	Two-channel PEC *I* + PEC *P* (one-sided)	160	382000	BM at 10 mm from the fusion line
12	Two-channel: PEC *I* + PEC *P* (doulbe-sided)	160	414000	Weld center
13	Two-channel: PEC *I* + PEC *P* (double-sided — weld + fusion line)	160	718000	Along the fusion line

Table 4 Results of fatigue tests of specimens of AMg6 alloy welded joints (Figure 4) at σ_a = 80, 120 and 160 MPa in the coordinates $2\sigma_a – N$ for single-channel scheme

Initial state — before EDT						
N	520000	470000	460000	210000	150000	130000	140000
$2\sigma_a$, MPa	80	80	80	120	160	160	160
After EDT						
N	1000000	1050000	1040000	560000	360000	390000	392000
$2\sigma_a$, MPa	80	80	80	120	160	160	160

N during the realization of EPE is also the deformation strengthening of the weld on the basis of electric stimulation, which explains the displacement of the fracture zone from the fusion line into the base metal.

It should be noted that namely at a small amplitude of the cycle $2\sigma_a$ = 80 MPa the level of residual welding stresses has the greatest effect on the value of N. When comparing the initial N (line 1) with its values obtained after EDT on one- (line 5) and two-channel (line 9) schemes of ED, the dominance of the latter as a tool that provides the greatest increase in N can be seen. At the same time, the preliminary cyclic loading, which helps to reduce the level of residual welding stresses before the beginning of EDT, provides an increase in N as compared to the specimens treated without a preliminary force effect. This fact gives grounds to assume that the preliminary load is the factor increasing the life of welded joints during the use of EDT, which in the future may be the subject of special investigations.

When comparing the effect on the life of EDT on a two-channel schemes of ED that realize the effect of PEC I (line 10) and PEC I + PEC P (line 9), it can be seen that the contribution of the current action increases N. The increase in the contribution of the current component into the electrodynamic effect, which is performed on the scheme PEC I + PEC P and intensifies the manifestation of the electroplastic effect, seems to be promising and quite simply realized on the considered element base.

The carried out investigations showed the effectiveness of EDT of AMg6 alloy and its welded joints in increasing the resistance to fracture under cyclic loads in the conditions of symmetrical bending. The use of EDT of the base metal [6], welded joints, as well as elements of thin-sheet structures in the area of expected fractures will allow increasing the service life of manufactured products and those, operating under cyclic loads.

Conclusions

1. It is shown that electrodynamic treatment (EDT) of specimens of butt welded joints of AMg6 alloy leads to a decrease in the level of residual tensile welding stresses, which is accompanied by their transition to compression stresses.

2. It was established that as a result of double-sided single-channel EDT of the surface of welded joints of AMg6 alloy, the cyclic life is three times increased as compared to the initial one. The additional EDT of the fusion line five times increases the life as compared to the untreated metal.

3. According to the results of comparative evaluation of single-channel and double-channel EDT of welded joints of AMg6 alloy, it was established that the increase in life during the use of a two-channel scheme (as compared to a single-channel one) is determined by a controlled synchronization of electrodynamic components, which excludes passing of PEC in the phase of its attenuation through the treated metal.

4. It was established that the life of the specimens treated on a two-channel scheme during electropulsed action, is more than 50 % higher than during dynamic action, which is associated with the contribution of the electroplastic effect in reducing the level of residual welding stresses.

1. Knysh, V.V. (2014) Determination of cyclic life of structure elements in arresting fatigue cracks. *The Paton Welding J.*, , 69–71.
2. Knysh, V.V., Klochkov, I.N., Pashulya, M.P., Motrunich, S.I. Increase of fatigue resistance of sheet welded joints of aluminium alloys using high-frequency peening. *Ibid.*, **5**, 22–29.
3. Finkel, V.M., Ivanov, V.M., Golovin, Yu.I. (1983) Crack healing in metals by crossed electric and magnetic fields. *Problemy Prochnosti*, **4**, 54–58 [in Russian].
4. Lobanov, L.M., Pashchin, N.A., Solomijchuk, T.G. et al. (2012) Changes of structure of AMg6 aluminium alloy in electrodynamic effects. *Visnyk Ukrainskogo Material. Tovarystva*, **5**, 30–42 [in Russian].
5. Lobanov, L.M., Pivtorak, V.A., Savitsky, V.V., Tkachuk, G.I. (2006) Procedure for determination of residual stresses in welded joints and structural elements using electron speckle-interferometry. *The Paton Welding J.*, **1**, 10–13.
6. Lobanov, L.M., Pashchin, N.A., Yashchuk, V.A., Mikhodui, O.L. (2015) Effect of electrodynamic treatment on the fracture resistance of the AMg6 aluminum alloy under cyclic loading. *Strength of Materials*, **3**, 91–98.
7. Yakovleva, T.Yu. (2003) *Local plastic deformation and fatigue of metals*. Kiev, Naukova Dumka [in Russian].
8. Baranov, Yu.V., Troitsky, O.A., Avramov, Yu.S. (2001) *Physical principles of electropulsed and electroplastic treatments and new materials*. Moscow, MGIU [in Russian].

PECULIARITIES OF PRODUCING LAYERED METAL COMPOSITE MATERIALS ON ALUMINIUM BASE

Ju.V. Falchenko, L.V. Petrushynets and **E.V. Polovetskii**
E.O. Paton Electric Welding Institute of the NAS of Ukraine
11 Kazymyr Malevych Str., 03150, Kyiv, Ukraine. E-mail: office@paton.kiev.ua

Analysis of publications devoted to producing layered composite materials on aluminium base was performed. The methods of joining thin-foil materials were studied, which allow producing layered joints with different number of intermediate layers. It is shown that the main welding methods, allowing production of joints with a layered structure, are rolling, ultrasonic, explosion and diffusion welding, and reaction sintering. Analysis of publications showed that the joining process can be conducted both in vacuum and in air. Joining foil from titanium and aluminium in the welding modes below the aluminium melting temperature (660 °C), allows producing joints without intermediate phase formation between the layers. In order to improve the strength of the produced composites, it is rational to apply during welding a technological operations in the form of current passing or postweld heat treatment of layered composite materials that provides increase of reactivity of the aluminium and titanium layers and formation of intermetallic phase as the reaction products. 31 Ref., 7 Figures.

K e y w o r d s : metal layered composite materials, joining methods, joint zone, intermetallic phase

When samples of new equipment are created, ever higher requirements are made of its weight and strength values that necessitate development of new materials which would satisfy this demand. Composite materials can be regarded as such.

Composite materials (CM) are those which have in their composition components insoluble or little soluble in each other, which differ essentially by their properties and which are separated by a clearly defined boundary in the material. CM properties mainly depend on physico-mechanical properties of the components and strength of the bond between them. A distinctive feature of CM is the fact that component advantages and not their disadvantages are manifested in them. At the same time, CM have properties, not found in the components which are included into their composition. In order to optimize the properties, components that differ markedly, but complement each other are selected [1].

CM properties depend on the shape and nature of filler distribution. By their geometrical shape, the fillers are divided into zero-dimensional, one-dimensional and two-dimensional (Figure 1). Zero-dimensional fillers have sizes of the same order in three dimensions (dispersion-strengthened CM). One-dimensional fillers consist of fibers of different intersections (fibrous CM), and two-dimensional fillers are plates, the length of which is greater than their thickness (layered CM) [2].

Layered composite materials (LCM) consist of rigidly connected metal or metal-containing alternating layers. These materials have a unique laminated structure with clear-cut interfaces and they can consist of layers of a broad range of materials. Depending on their thickness, the composite layers can be classified as sheets or plates of 1–10 mm and greater thickness, foils of 0.05–1.0 mm thickness and films of 0.001–0.05 mm thickness [3]. LCM can greatly improve a number of properties, including fracture toughness,
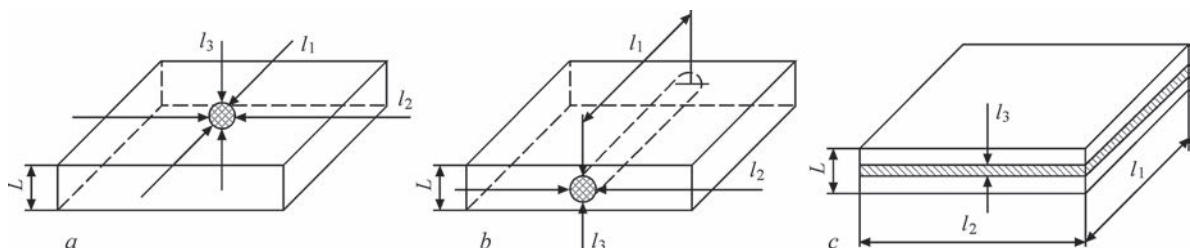

Figure 1 Forms of fillers: *a* — zero-dimensional; *b* – one-dimensional; *c* — two-dimensional: l_1; l_2; l_3 — filler dimensions; L — matrix thickness [2]

Ju.V. Falchenko — https://orcid.org/0000-0002-3028-2964, L.V. Petrushynets — https://orcid.org/0000-0001-7946-3056,
E.V. Polovetskii — https://orcid.org/0000-0002-8113-0434

fatigue characteristics, impact characteristics, wear, corrosion and damping ability, and provide higher ductility of brittle materials. Selection of component materials and their volume percent, layer thickness, and respective treatment, allows producing a material with specified properties [4].

LCM with a hard matrix and soft filler, are mainly applied as high-temperature materials, and those with a soft matrix and hard filler are used as heat-resistant materials. By functional characteristics LCM are divided into: corrosion-resistant, antifriction, electrical engineering, tool, wear-resistant, thermobimetals, bimetals for deep drawing and household products [3].
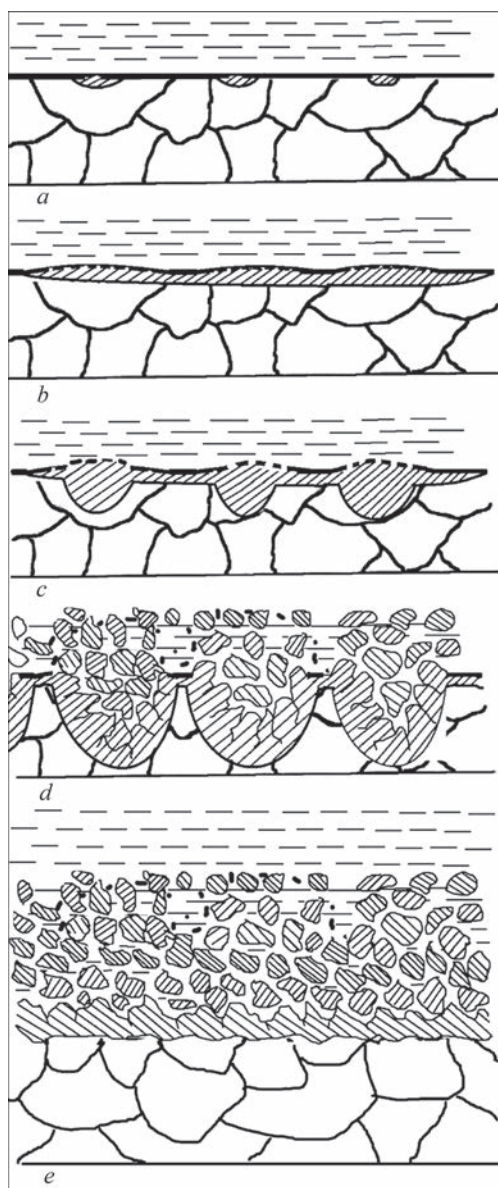

Fig re 2 Mechanism of transformation of the microstructure of VT1-0/AD1 layered composite during heat treatment at temperatures above aluminium liquidus point: *a* — aluminide nuclei formation; *b* — transverse growth of thin interlayer sections; *c* — formation and acceleration of the growth of intermetallic phase nuclei in the zones of channels between oxide film fragments; *d* — intermetallic fragmentation; *e* – appearance of a continuous band of intermetallic fragments coated by a film of Al melt [5]

Considering that aluminium and titanium are some of the lightest metals, and are widely applied in different industries, the objective of this work was performing analysis of the methods to produce LCM based on aluminium and titanium.

The methods to produce LCM can be conditionally divided into those, where materials are formed in the solid or liquid state by welding methods, as well as through gaseous condition or solution by deposition methods. The following can be included into the first group: joining by melt impregnation techniques, sintering, rolling, ultrasonic, diffusion and explosion welding. The second group includes: thermal spraying, evaporation and vapour phase deposition in vacuum, methods of chemical deposition of metal from melts.

Let us consider producing layered composite materials by welding methods.

LCM manufacture by **melt impregnation method** implies contact of liquid filler metal with the solid metal of the matrix. The authors [5] proposed a mechanism of running of the processes of aluminium melt interaction with solid titanium (Figure 2), in keeping with which the aluminium melt is not directly contacting titanium initially, as Al_2O_3, TiO_2 (or TiO) interlayers are located between them. The process of titanium and aluminium atom diffusion through the interface in the presence of oxide films is slowed down. That is why it predominantly occurs along the ruptures of oxide films with appearance of local areas of oversaturated solid solution of Ti(Al) in titanium with further formation of nuclei of Al_3Ti intermetallics. This is followed by transverse growth of aluminides up to their coalescence with formation of a continuous interlayer along titanium.

Oxide film fragmentation promotes diffusion of aluminium atoms from the melt to the titanium surface, thus promoting formation and accelerated growth of intermetallic phase nuclei. Intermetallic formation in the volume limited by titanium which has reacted, leads to further breaking up of the oxide film, abrupt increase of internal stresses and breaking up of the formed aluminides into individual fragments, and their ousting from the reaction volume. This facilitates access of the aluminium melt practically to the reaction surface and promotes acceleration of the processes of localized growing of intermetallics right up to their closure and formation of a continuous strip of aluminide fragments, coated by a film of aluminium melt. Fragments of intermetallics that broke off, are inactive, and stay near the reaction surface, from which they are driven by new fragments that form constantly.

Work [6] is a study of the impact of liquid phase temperature on LCM formation. The materials used were commercial aluminium A7 and VT1-0 titanium

of 40×40×0.5 mm size. The gap between the titanium layers was 0.125–0.7 mm. Titanium was first etched for 5–10 min at 20 °C in the following solution: 1 l of water, 20–30 ml H_2NO_3 and 30–40 ml HCl. Flux of KF–AlF_3 system was used for surface activation. Temperature of aluminium melt was set in the range of 670–950 °C. It was found that the wetting level practically does not change at increase of melt temperature and reaches the maximum value at 700–750 °C. The highest values of wetting level, as well as better mechanical properties in the entire studied temperature range were obtained for joints with 0.35 mm gap between the titanium layers ($\tau \approx$ 65–80 MPa). During LCM formation a two-phase zone is created between Al and Ti layers, which consists of aluminium (Al and up to 0.5 % Ti) and titanium (Al_3Ti) phases. Here, the quantity of the intermetallic phase increases with process temperature. At 800 °C a continuous interlayer of Al_3Ti forms between aluminium and titanium.

When LCM are manufactured by **plasma sintering** method, pulsed direct current is used as the heat source. Here, the material in the impact zone can be heated up to high temperatures, right up to plasma state.

In work [7], layered titanium-aluminium composite was produced by the method of plasma sintering of aluminium and titanium foil of 26 mm diameter, 100 and 200 μm thick, respectively. Total number of foils in the pack was 70 pcs. The process was conducted at the temperature of 830 °C, pressure of 5.7 MPa, and 1–5 min duration. Partial pressing out of molten aluminium from the pack, as well as plastic deformation of titanium lead to reduction of sample thickness by 10–30 %. Process performance results in formation of layered Ti−Al_3Ti intermetallic composite. Increase of soaking time up to 50 min, allows reducing porosity in titanium aluminide layers, as well as increasing their hardness from 2.9 up to 3.8 GPa.

In order to obtain the layered structure, the authors of [8] also used plasma sintering. Investigations were conducted with foil of commercial aluminium and titanium of 27 and 45 μm thickness, respectively, and 15 mm diameter. Foil was cleaned in an ultrasonic pool in methanol and assembled in a pack of 40 Al discs and 41 Ti one. Spark plasma sintering was conducted under vacuum of 10^{-3} Pa at direct current of 1.0–1.5 kA, voltage of 5–10 V; pulse frequency changed in the range of 30–40 kHz. The pack was first sintered at the temperature of 450 °C, pressure of 50 MPa, and soaking for 10 min. This was followed by annealing at 900 °C, for 30 min in an argon atmosphere. Final sintering was performed in the temperature range of 950–1200 °C at heating rate of up to 100 °C/min, pressure of 50 MPa, at soaking for 10 min. Preliminary sintering resulted in for-

mation of a layered structure without any noticeable interaction of Al and Ti. After annealing the binary structure is transformed into the following interlayers: α-Ti, $AlTi_3$, AlTi, Al_2Ti and thick layer of porous Al_3Ti. Al melting, Kirkendale effect and difference in molar volumes between the reagents and products are indicated as the causes for formation. The second sintering cycle allows almost complete healing of pores. At process temperature of 950 °C the following layer composition forms: α-Ti, $AlTi_3$, AlTi, $Al_{11}Ti_5$ and Al_3Ti. Further temperature rise leads to reduction of the number of layers. So, α-Ti, $AlTi_3$, AlTi were obtained at 1050 °C, and a homogeneous mixture of $AlTi_3$ with AlTi was produced at 1200 °C. It was also established that the bending strength of layered samples produced at 950 °C is more than three times higher than that of samples sintered at 1050–1200 °C ($\sigma_{t\ bend}$ = 1400 MPa against $\sigma_{t\ bend}$ = = 389–446 MPa). This is accounted for by availability of α-Ti layer, which deformed plastically and prevented crack propagation in the direction normal to the composite layer plane, promoting crack deviation and branching. Such a microstructure absorbs a large amount of energy before breaking.

In work [9] reaction sintering of a foil pack from VT00 and A5E alloys (100×10×0.05 mm) was performed. The first and last layers were from titanium. Total thickness of the pack was 1 mm. Foils were first processed in 2 % solution of hydrofluoric acid. The pack was placed between ceramic plates and heated up to 630 °C in a heat-resistant box at the rate of 15 °C/min. Current was passed with a frequency of 40, 800 and 1600 Hz. The best results were obtained at application of unipolar pulses («−» was connected to Ti layers, «+» was connected to Al). It was found that at heating without current passage, complete transformation of the pack into Ti−Al_3Ti LCM occurs in 420–480 min. Additional passage of current reduces the time of layered composite formation to 300 min. During sintering, just Al_3Ti intermetallic forms. Its formation leads to appearance of pores and microcracks at the start of chemical transformation. Before completion of the sintering process, the discontinuities heal under the impact of pressure so that the final structure of layered composite is an alternation of residual Ti layers 30–35 μm thick and Al_3Ti layers with microhardness of 4.5–7.0 GPa.

The authors of [10] proposed a procedure of calculation of process parameters and scheme of layer transformation when producing titanium-aluminium LCM at direct current passage. Aluminium and titanium foils (90×10×0.05 mm) were assembled in a pack of the total thickness of 1 mm. The first and last layers were from Ti. Sintering was conducted at the temperature
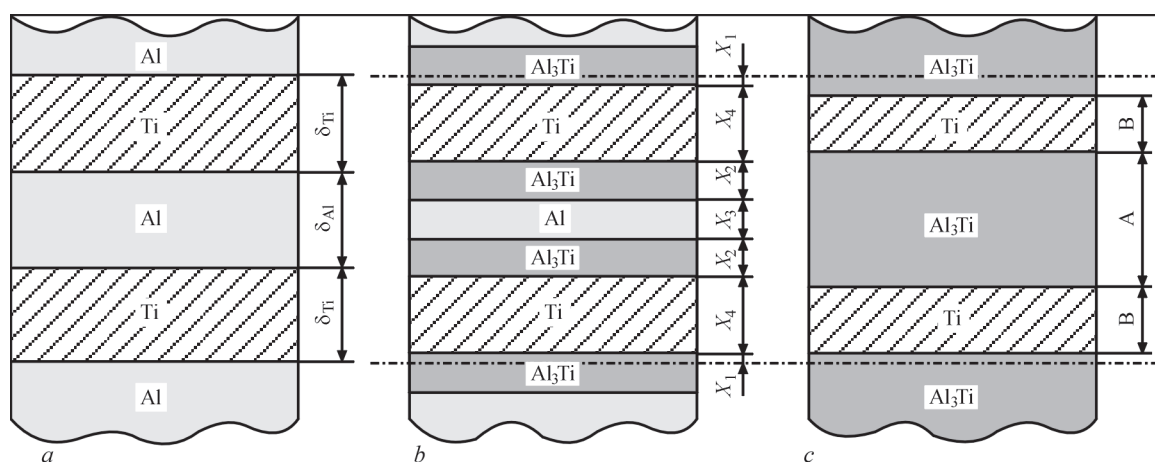
Figure 3 Scheme of transformation of layers in a pack of Al and Ti foils: *a* — initial state; *b* — intermediate state; *c* – process completion [10]

of 630 °C and pressure of 25 MPa. Figure 3 gives the scheme of transformation of layers in a pack of Al and Ti foils. The work presents a procedure of calculation of the parameters of current processing of a multilayer pack to obtain metal-intermetallic Ti−Al_3Ti LCM. Selection of boundary values of current that allow reducing the time of pack processing without partial melting of the aluminium layers, was substantiated. For the considered case the current is 150 A.

One of the most widespread methods of LCM manufacturing is **rb ling**, which consists in joint rolling of a pack of metal layers.

The authors of [11] used the rolling method to obtain layered titanium-aluminium composite. For this purpose, they assembled a pack of plates from VT1-0 alloy (100×50×0.1 mm) and AD1 alloy (100×50×0.02 mm). The following thickness ratios of titanium and aluminium layers were selected: 100/20, 100/40, 100/60, 100/200 (μm). Rolling was conducted in steel sheaths at the temperature of 450–520 °C under a vacuum of 0.01 Pa. At the first passage the degree of deformation was equal to 25–40 %, at the following passes it was 8 to 10 %. As a result strips of 0.35 mm thickness with 4800 layers were produced. Here, the average thickness of the titanium layer was 100–120 nm, and that of the aluminium layer was 80–90 nm. Deformation of aluminium layers was by 25–30 % greater than that of titanium layers. It led to violation of the continuity of the titanium layer. Deformation of the subsurface layers of both the materials was by 10 to 15 % greater than that of the central layers. Experimental results allowed establishing an optimum rolling temperature (470 °C) and degree of cogging in rolling (up to 30 % in one pass), which allow welding the Ti and Al layers, and prevent formation of more than 0.5 % of intermetallic phases in the composite.

In work [12] a pack of two foils from AA1235 aluminium 300 μm thick and one titanium foil 25 μm thick was rolled at room temperature. The total thickness of the pack was reduced from 625 to 130 μm. Here, the titanium layer was broken up and dispersed in the aluminium matrix. This was followed by annealing the samples at 600 °C for 3600–10080 min with the purpose of formation of Al_3Ti intermetallic. At less than 720 min duration of heat treatment pores are observed (Kirkendale effect) on Al/Al_3Ti interface, because of a significant difference in Al and Ti diffusion. Pore presence leads to lowering of the values of ductility and strength of the composite sheet. Increase of annealing time to 1440 min promotes healing of pores, composite material consists of coarse-grained particles of Al and ultradispersed Ti and Al_3Ti. In this case also higher values of mechanical properties (σ_y = 135 MPa) are achieved. At annealing duration of 2880 min, pure Ti disappears with its complete transition into Al_3Ti. At further increase of annealing time to 10080 min, Al_3Ti particles are redistributed in Al matrix closer to LCM surface that leads to lowering of strength and ductility.

The authors of work [13] joined Al and Ti foils by the method of rolling at room temperature. After scraping by a metal brush and in acetone, the foils were assembled into a pack of 100×50 mm that consisted of layers of titanium 82 μm thick and aluminium 80–140 μm thick. It was found that the deformation level is almost the same for all LCM layers. However, bonding of the pack central layers occurs earlier than that of the external ones, which is caused by elastic recovery of the external layers that leads to breaking up of the bonds formed after passing under the rolls. Presence of scratches on aluminium after scraping leads to increase of the coefficient of friction on layer interfaces that promotes an increase of adhesion strength at the initial stage of the process and reduction of soft metal pressing out on the pack edges. Experimental results also showed that when a thinner aluminium layer (80 μm) is used, its thickness decreases

significantly, compared to the initial value. Increase of Al thickness allows producing LCM with a more uniform change of relative thickness of both the metals, and aluminium extrusion is minimized (Figure 4).

Work [14] is a study of dislocation formation in aluminium at long-term annealing of Al/Ti/Al LCM. AA1235 aluminium foil 300 μm thick and pure titanium 25 μm thick were used for producing LCM. Cold rolling of a pack of three foils was performed in a four-roll mill with 50 mm diameter rolls. Total thickness of the pack was reduced from 625 to 130 μm. Rolling was followed by annealing of the produced joints at 600 °C for 360–10080 min. Heat treatment promotes Al and Ti diffusion to the interface and a reaction between them with formation of Al_3Ti intermetallic. Kirkendale effect and difference in molar volumes of the reagents results in pore formation on Al and Al_3Ti interface. Increase of annealing duration to 2880 min leads to a significant decrease of pore size. At heat treatment for 10080 min, anomalously high dislocation density of $7.5 \cdot 10^{14}$ m^{-2} is observed in Al layer near Al_3Ti intermetallic. The authors state that this is caused by development of pores and diffusion of Ti atoms. Interdiffusion of Ti and Al and Al_3Ti formation at long-term annealing of strongly deformed material allows some Ti atoms going beyond Al_3Ti stoichiometry limits and forming a buffer zone that consists of Ti solid solution in Al. With longer annealing time, large pores separate into smaller ones and are distributed in the aluminium matrix. Movement of atoms at a high temperature promotes gradual decrease of spherical pore size, which become vacancies as a result of it. In addition, in order to minimize free energy, the distributed Ti atoms were gathered in vacancies, and dislocations were formed and pinned by Ti atoms and clusters.

Ultrasonic welding belongs to solid-phase methods and envisages use of ultrasonic oscillations as the energy source, alongside pressure application. This process allows joining a wide range of metals up to 3 mm thick. Welding takes place at low temperatures that allows producing the joint without intermetallic formation.

The authors of [15] performed ultrasonic welding of an Al/Ti pack into LCM. A substrate from AA1100 aluminium alloy 1.5 mm thick was used as the first layer. Foil from pure titanium and AA1100 aluminium 127 μm thick was selected for the experiments. The foils were alternately assembled into a pack of 2–10 layers. Up to four foils were joined in one pass. Welding was followed by heat treatment at 480 °C for 240 min. It was found that rupture strength rises with increase of the total number of layers and reaches $\sigma_t = 216$ MPa for LCM of 10 layers that is attributable to
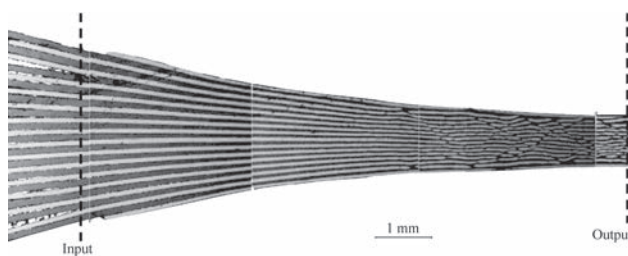

Figure 4 Cross-section of Al/Ti LCM produced by the rolling method [13]

increase of volume fraction of titanium. Layered material ductility also rises with increase of the number of layers up to 6 ($\delta = 32$ %), and after that it almost does not change.

Work [16] was a continuation of previous studies. Welding, however, was performed already without backing. Pure titanium and aluminium of 1100 grade up to 127 μm thick were used in the experiments. Foils were alternately assembled in packs with the total number of 7 to 15 layers, the first and last of which were from titanium. Samples were joined with a certain force and at sonotrode frequency of 20 kHz. Welding was performed in several stages, depending on the number of layers. First a pack of three foils of Al/TI/Al was assembled and passed under the sonotrode. This was followed by adding two more foils of Al + Ti and the process was repeated. Then annealing at 480 °C was performed for 240 min, in order to improve the joint quality. Increase of the number of layers has a negligible influence on mechanical characteristics of the joints. However, better results were obtained for a pack of 15 foils that is attributable to a greater number of passes in welding under the sonotrode.

The authors of work [17] studied the features of LCM joint formation under the impact of ultrasonic welding. Three foils from pure titanium and three from aluminium 1100 of 127 μm thickness each were used for this purpose. Welding was performed in Fabrisonic SonicLayer 4000 system of 9 kW power at the following parameters: 3500 N compressive force, 41.55 μm vibration amplitude, and 25.4 mm/s welding speed. In order to increase the ductility and intensify the adhesion process, the substrate from aluminium alloy 6061 was heated up to 93.3 °C. One titanium foil and one aluminium foil were welded in one pass. Discontinuities are observed on the interfaces between the individual layers. There are no intermetallics in the joint zones. During welding, mainly aluminium is deformed, that is indicated by grain disorientation by 9°, and more than two times reduction of their size at almost unchanged values for titanium. A conclusion was made that the main mechanism re-

sponsible for joint formation in ultrasonic welding is strong shear deformation on the layer interface.

Further studies were devoted to determination of the impact of heat treatment on the joint and they are covered in work [18]. The alloys and parameters of ultrasonic welding modes were the same as in the previous work. Joint samples were subjected to annealing at 600 °C for 60 min. Sound joints were produced, where considerable growth of grains in the aluminium layer and formation of a thin intermetallic interlayer on Al/Ti interfaces took place. Delamination testing results showed that the force required for sample breaking after heat treatment, is almost two times higher than that directly after welding (5.8 kN against 2.4 kN). Here LCM breaking after welding takes place within one layer, and in the annealed samples it runs through several layers that is indicative of higher joint strength along the layers, compared to the initial materials. Shear strength studies showed the same tendency of values — τ_{sh} = 46.3 MPa, after welding and τ_{sh} = 102.4 MPa for heat-treated LCM.

In work [19], the impact of heat treatment on mechanical properties of LCM produced by the method of ultrasonic welding was studied. Foil from 3003-N18 aluminium alloy 150 μm thick and pure titanium 75 μm thick was used. LCM was built up layer-by-layer on a massive substrate from 3003-N18 alloy, starting from titanium. The mode of welding aluminium foil was as follows: compressive force of 1750 N, vibration amplitude of 16 μm, welding speed of 23.7 mm/s; for titanium foil it was: compressive force of 2000 N, vibration amplitude of 28 μm; welding speed of 10.58 mm/s. Preheating temperature was 150 °C in both the cases. Then annealing at 480 °C was conducted for 30–270 min. The method of optical metallography showed continuous contact between Al and Ti, and no defects were found in the joint zone. Heat treatment for 30 min allows reliev-

ing the stresses, that arose between the metal layers during welding, and almost two times increasing the shear strength, compared to unannealed samples (τ_{sh} = 72.96 MPa against 37.78 MPa). Increase of soaking duration at annealing leads to recrystallization and growth of the grains, resulting in a drop in strength.

Application of **diffusin welding** allows at the initial stage of the process localizing plastic deformation of matrix material, required for filling the space between the layers of the strengthening phase and for maximum densification of the matrix proper. When tight contact occurs between the layers, diffusion processes run on the interface, which provide strong bonding on these interfaces, and required strength level of the CM proper.

The authors of work [20] joined by diffusion welding the foils from TA1 titanium and 1060 aluminium alloys of 220×220×0.1 mm size. First 1 MPa pressure was applied to the samples in a vacuum furnace, to ensure tight contact between Al and Ti layers. Then, heating up to 500 °C was conducted for 180 min with soaking for 60 min at this temperature, to ensure uniform heating of the foil. Then temperature was increased up to 550 °C for another 30 min, and samples were soaked for 180 min to achieve diffusion welding of the layers, here pressure was increased up to 3 MPa. Finally, the foil was cooled together with the furnace under pressure of 1 MPa. Thus, LCM without pores or intermetallic inclusions on Al and Ti interfaces was produced (Figure 5).

Work [21] indicates the need for prior degassing of the foil in LCM production. The authors used foil from AM5 aluminium and VT1-0 titanium of thicknesses of 50 and 100 μm, respectively. Foil was rinsed in acetone, alternately assembled into a pack and heated up to 640 °C for 30 min in the vacuum of 1.333 Pa to ensure degassing. Rather intensive gas evolution is indicative of vacuum deterioration at this stage by an
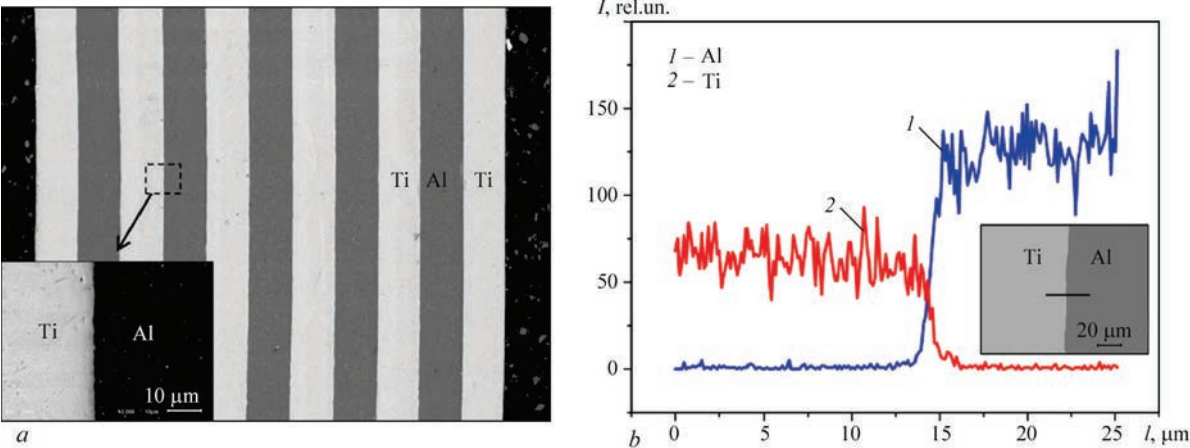

Fig re 5 Cross-section (*a*) and distribution of elements in the joint zone (*b*) of Al/Ti LCM, produced by the method of diffusion welding [20]

order to 13.33 Pa. Then, the samples were compressed with a certain force and soaked at the same temperature for another 240 min. It resulted in producing Ti/Al$_3$Ti LCM. Here, a large number of microcracks and pores in place of the former aluminium foil are observed in the intermetallic layer.

In work [22], the method of diffusion welding was used to produce LCM from 1060 aluminum alloy 100 μm thick and TA1 titanium alloy 150 μm thick. Welding was performed in the following mode: 550 °C temperature, 5 MPa pressure, 180 min process duration and 10^{-3} Pa vacuum. To endure tight contact of the foils, pressure was applied before heating. Cooling to room temperature was performed together with the furnace. LCM without pores, discontinuities or intermetallic inclusions with ultimate strength σ_t = 224 MPa and relative elongation δ = 35 % was produced. Results of bend testing showed that microcracks on Al/Ti interface appear at bend angle of 120°. No sample bending occurs even at its bending up to 180°.

The authors of [23] studied the impact of thickness of aluminium and titanium foil on LCM formation by diffusion welding. Pure titanium (0.15–0.4 mm thick) and AA1060 aluminium (0.1–0.4 mm thick) were used as investigation materials. Al and Ti foil was cut up into 300×300 mm squares. Initial thickness ratio of Al and Ti layers was as follows: 0.1/0.15, 0.2/0.25, 0.4/0.4. Total pack thickness was 1.15–1.2 mm. Before welding, Ti was etched in a solution, consisting of 35 % nitric acid, 5 % fluoric acid and water. Aluminium foil was first cleaned in alkali solution of 30 g/l sodium hydroxide heated up to 50–60 °C, which was followed by immersion in an aqueous solution of nitric acid of 300–350 g/l at room temperature. Then samples were washed in water, then in ethanol. Diffusion welding was conducted in the following mode: 550 °C temperature, 5 MPa pressure, and 180 min soaking under the conditions of 10^{-2} Pa vacuum. Cooling to room temperature was performed in the furnace. Metallographic investigations showed that at reduction of the layer thickness the interface between them becomes wavelike. It results in increase of the total area of the surface of contact between the metals, compared to the initial condition. Reduction of layer thickness ratio from 0.4/0.4 to 0.1/0.15 also promotes increase of the diffusion zone from 4.1 up to 5.2 μm. Samples with thickness ratio of 0.4/0.4 (σ_t = 288.03 MPa) had the maximum tensile strength, however delamination between titanium and aluminium is absent only in 0.1/0.15 samples (σ_t = 223.67 MPa).

In work [24] previous studies were continued with a focus on investigation of the process of initiation and propagation of a fatigue crack in LCM. Al and Ti foils of 0.15 and 0.1 mm thickness, respectively, were used. Diffusion welding was performed in the following mode: 500–600 °C temperature, 5 MPa pressure, 180 min soaking duration, and 10^{-3} Pa vacuum. Sound joints without intermetallic inclusions and with higher mechanical properties were produced at welding temperature of 550 °C (σ_t = 224 MPa). After 67554 loading cycles fatigue cracks appear on sample edges. Their initiation mechanism is considerable local plastic deformation resulting from high stress concentration. Fatigue cracks propagate mainly normal to the loading direction. During their propagation, large triangular cracks form, and fatigue cracks spread in several directions, forming a large number of microcracks. This is followed by interphase delaminations, which prevent further initiation and propagation of the fatigue cracks and release the fatigue cycle stresses. Threshold value of fatigue crack propagation in Al/Ti LCM was close to 7.4 MPa·m$^{1/2}$ that is higher than that in titanium and aluminium.

Work [25] is a study of the process of initiation and growth of Al$_3$Ti intermetallic phase between Al and Ti layers in diffusion welding with further annealing. Used for this purpose were aluminium and titanium sheets of 0.5 mm thickness. Before welding the samples were cleaned in an ultrasonic bath in 10 % solution of hydrofluoric acid. Aluminium and titanium sheets were stacked alternately up to the total thickness of 5 mm, pressed together with 4 MPa force, heated up to 550–575 °C and soaked for 120–360 min. Annealing was conducted at the welding temperature for 720–2880 min. After welding of 360 min duration a thin Al$_3$Ti interlayer forms in the joint zone, the thickness of which becomes greater during subsequent annealing. After heat treatment at 575 °C for 2880 min the aluminium layer disappears completely. It was found that at annealing at 575 °C for 2160 min Al diffusion rate is 20 times higher than that of Ti (D_{Al} = 27.133·10^{-15} m^2/s against D_{Ti} = 1.202·10^{-15} m/s). It leads to pores formation near Al/Al$_3$Ti interface, as a result of Kirkendale effect. Such predominating diffusion of Al towards Ti stimulates initiation and growth of the intermetallic phase mainly on Ti/Al$_3$Ti interface. Figure 6 gives the scheme of Al$_3$Ti growth under the impact of temperature. During welding diffusion of individual Al and Ti atoms takes place with formation of Al$_3$Ti phase along Al/Ti interface (Figure 6, *b*). Annealing is accompanied by non-uniform growth of the intermetallic phase (Figure 6, *c*): ultrafine Al$_3$Ti (A) grains form near Ti, grains with coarse structure (B) form in the central part of Al$_3$Ti layer, and relatively small Al$_3$Ti grains (C) appear near the aluminium layer. This is caused by a high level of aluminium diffusion that promotes more in-
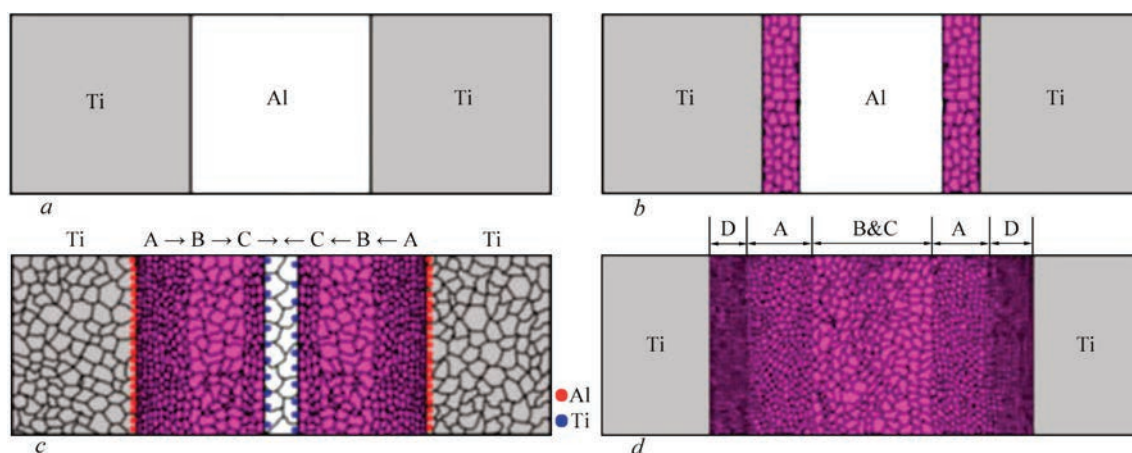
Fig re 6 Schematic image of the process of Al₃Ti growth in Al/Ti layered system: *a* — initial stage; *b* — intermediate state; *c* — final structure after Al transition into intermetallic [25] (for A, B, C, B description see the text)

tensive formation of intermetallic phase nuclei on Ti/Al₃Ti interface with shifting of regions A, B, and C towards the aluminium layer. After complete transition of Al into the intermetallic, regions B and C mix in the central part of the intermetallic layer (Figure 6, *d*). Thus, the final structure of Al₃Ti grain consists of recently grown fine Al₃Ti grains on Ti/Al₃Ti interface (D), region A with a certain coarsening of the grains is shifted towards Al, that is adjacent to region D and mixed regions B and C in the central part.

The authors of work [26] studied reaction diffusion in a multilayer Al/Ti pack. Experiments were conducted with a pack of 17 titanium and aluminium foils of 90×25 mm size. Foils from Al and Ti were first etched in 10 % solution of hydrofluoric acid and 15 % solution of sodium hydroxide with further cleaning with alcohol and rinsing in water. Joining was performed at 600 °C temperature, 50 MPa pressure for 180 min under a vacuum not lower than 10^{-2} Pa. Then the produced samples were annealed at 520–650 °C for 60–9000 min. It was found that at heat-treatment in the selected temperature range Al₃Ti is a single phase that is observed in the diffusion zone. Titanium and aluminium diffuse in the direction towards each other. Al₃Ti layers, however, grow mainly towards Al. At 575 to 600 °C temperature, the kinetics of Al₃Ti growth changes from the parabolic to linear one. In low-temperature kinetics, diffusion of Ti atoms along the grain boundaries of Al₃Ti layers prevails, whereas the reaction on the Al/Al₃Ti interface in the high-temperature mode is limited by diffusion of Ti atoms into Al foil on Al₃Ti growth front, as a result of higher solubility of Ti in Al with temperature rise.

In work [27] the impact of titanium thickness on formation of Al/Ti LCM was studied. Titanium of 45–180 μm thickness and aluminium of 54 μm thickness were used. Foil of 40×80 mm size was scraped with a wire brush and cleaned in alcohol in an ultrasonic bath. Then 50 Ti layers and 49 Al layers were alternately stacked in a graphite matrix. Welding was conducted in a vacuum furnace in the following mode: 500 °C temperature, 50 MPa pressure, soaking for 30 min. Then, the produced sample was annealed without applying pressure at 900 °C for 30 min for complete transition of aluminium into the intermetallic phases. Final sintering was performed in high vacuum of the order of 10^{-3} Pa at 1050 °C, under a pressure of 50 MPa for 60 min, heating rate was 10 °C/min, and cooling rate was about 15 °C/min. After all the stages of thermodeformational impact, joints with slight porosity were produced. Irrespective of titanium thickness, the following sequence of phase layers formed: α-Ti, AlTi₃, AlTi, Al₂Ti and Al₃Ti. Samples produced with titanium of 90 μm thickness had the highest tensile strength (σ_t = 606 MPa) and fracture toughness (K_{1C} = 47.6 MPa·m$^{1/2}$). This is attributable to optimum ratio (almost one to one) between α-Ti and total thickness of intermetallic layers. Such a volume fraction of α-Ti layers effectively prevents continuous crack displacement in the opening mode, making it deviate and bifurcate in the intermetallic layers. Plastic deformation of titanium may absorb a large amount of energy up to material fracture.

Ep lo in welding has limited application for LCM production. It is solid-phase process of producing the joints with intensive plastic deformation of metal under the impact of a short high-amplitude pulse.

In work [28] explosion welding was applied to produce Al/Ti LCM. VT1 titanium and aluminium (Al−1Mn) alloys of 100×200×0.2 mm and 100×200×0.25 mm size, respectively, were used as research materials. The sheets were alternately placed into a pack with the total number of 40 pcs. Ammonite powder 6GV of 0.9 g/cm³ density and 4200 m/s detonation rate was used as explosive. Further heat
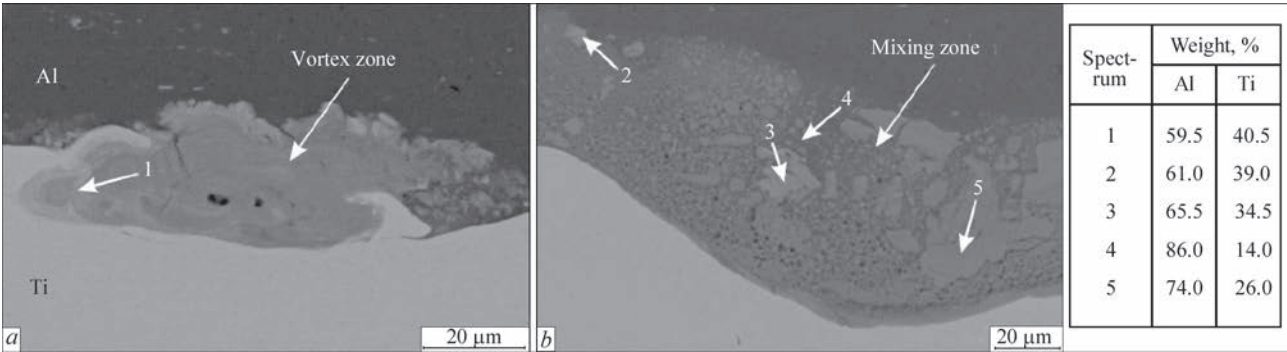
Spectrum	Weight, %	
	Al	Ti
1	59.5	40.5
2	61.0	39.0
3	65.5	34.5
4	86.0	14.0
5	74.0	26.0

Figure 7 Structure and chemical composition of mixing zones formed after explosion welding of Al/Ti LCM: *a* — vortex; *b* — dispersed inclusions (marked by arrows) [28]

treatment was conducted in air atmosphere at the temperature of 640 °C, and pressure of 3 MPa for 1200 min. In the produced samples a change of the joint zone between the aluminium and titanium layers from the wavelike to almost straight one is observed with greater distance from the explosion epicenter. Nonuniformity of the impact of explosion wave is the cause for presence of micropores between the individual layers. The following intermetallic phases form in the mixing zones: Al_3Ti, $AlTi$, Al_5Ti_3, and $AlTi_3$ (Figure 7). Further LCM heat treatment led to growth of Al_3Ti, the growth rate of which was four times higher, compared to samples made by the sintering technology. Pressure application at annealing allows producing samples with minimum number of defects.

Authors of works [29, 30] used explosion welding to produce a pack of six aluminium and titanium sheets 0.5 mm thick. A mixture of ammonium nitrate with trotyl and gas oil 20 mm thick was used as the explosive. The detonation rate was approximately 4500 m/c. Then LCM samples were annealed at 630 °C for 60–15600 min in ambient atmosphere. After welding the aluminium and titanium joint zone is a straight line without vortices. In some places, regions with Al_3Ti are observed between Al and Ti, formation of which is related to local temperature rise in welding. During the first 780 min at annealing the rate of intermetallic layer growth is of a linear nature, and after that its behaviour changes to a parabolic one. This is indicative of transition of Al_3Ti growth mechanism from controlled reaction to controlled diffusion.

In work [31], Al/Ti bimetal was produced from rather thick sheets by explosion welding method. Plates from Ti Gr. 2 titanium (140×460×0.8 mm) and A1050 A aluminium (140×460×4 mm) were used for this purpose. The distance between the metals before the explosion was 1.5 mm, and the detonation rate was 1900–1950 m/s. Then, the samples were annealed in sealed quartz ampoules at 552 °C for 30–6000 min. After welding sound joints were produced. The zone of aluminium and titanium joint acquires a wavelike

appearance, in the vortices of which Al_3Ti, Al_2Ti, $AlTi$ and $AlTi_3$ intermetallics form. The annealing process makes Al_3Ti phase the dominating one, promoting growth of its layer over the entire joint surface. Investigations of the kinetics of Al_3Ti intermetallic revealed four stages of its growth: incubation period (up to 90 min); growth controlled by a chemical reaction (90–300 min), mixed mechanism of the chemical reaction and volume diffusion (300–2160 min); and volume diffusion (2160–6000 min). Intensive growth of aluminium grains occurs during heat treatment.

Conclusions

Based on the presented review of publications, we can state that:

1. Application of LCM can greatly improve the properties of structures made from them, namely fracture toughness, fatigue and impact characteristics, wear, corrosion and damping ability.

2. Process of joining aluminium to titanium can be conducted both under vacuum, and in air. Here, depending on the final product, it is possible to produce LCM both with strengthening due to formation of intermetallic interlayers, and without it.

3. The main methods of producing LCM, based on aluminium and titanium is melt impregnation, rolling, sintering, ultrasonic, explosion and diffusion welding.

4. Each welding process has its characteristic features. The melt impregnation method envisages contact of liquid aluminium with solid titanium and does not allow producing LCM without the intermetallic interlayer. The rolling process requires considerable plastic deformation of the pack to obtain the laminates that leads to a considerable number of the rolling cycles. Ultrasonic welding is used only to produce a layered pack of thin foils. Explosion welding is accompanied by formation of a wavelike joint zone and requires further heat treatment. Diffusion welding, depending on welding mode parameters, allows producing LCM both with formation of the intermetallic phase in the butt joint, and without it.

Proceeding from the possibilities of wide adjustment of LCM structure and composition at the stage of forming the joint by diffusion welding, it is urgent to perform further investigations on production of such materials with controlled content of the intermetallic phase in the butt joint.

1. Arzamasov, B.N., Makarova, V.I., Mukhin, G.G. et al. (2008) *Materials science:* Manual for higher education instit. Moscow, N.E. Bauman MGTU [in Russian].

2. Tyalina, L.N., Minaev, A.M., Pruchkin, V.A. (2011) *New composite materials*: Manual. Tambov, GOU VPO TGTU [in Russian].

3. Kovtunov, A.I., Myamin, S.V., Semistenova, V.V. (2017) *Layered composite materials*: Electron manual. Tolyatti, TGU [in Russian].

4. Wadsworth, J., Lesuer, D.R. (2000) Ancient and modern laminated composites – from the great pyramid of gizeh to Y2K. *Materials Characterization*, **5**, 289–313.

5. Gurevich, L.M. (2013) Mechanisms of structure formation at interaction of titanium with aluminium melt. *Izvestiya VolgGTU, Seriya Problemy Materialovedeniya, Svarki i Prochnosti v Mashinostroenii*, **6**, 6–13 [in Russian].

6. Kovtunov, A.I., Myamin, S.V. (2013) Investigation of technological and mechanical properties of layred titaniumaluminium composite materials produced by liquid-phase method. *Aviats. Materialy i Tekhnologii*, **1**, 9–12 [in Russian].

7. Kuzmin, K.A., Lazurenko, D.V., Mats, O.E. (2014) Formation of «titanium−titanium aluminide» composite materials by the method of spark plasma sintering. In: *Proc. of 1st Int. Sci.-Pract. Conf. on Actual Problems in Machine-Building (Novosibirsk, 26 March 2014)*. Novosibirsk, NGTU, 514−520.

8. *Yanbo* Sun, Sanjay Kumar Vajpai, Kei Ameyama, Chaoli Ma (2014) Fabrication of multilayered Ti–Al intermetallics by spark plasma sintering. *J. of Alloys and Compounds,* **5**, 734–740.

9. Sinchuk, A.V., Tsurkin, V.N., Ivanov, A.V. (2016) Effect of electric current on reaction sintering of Ti–Al layered system. *Konstruktsii iz Kompozitsionnykh Materialov*, **1**, 24–31 [in Russian].

10. Vasyanovich, N.A., Tsurkin, V.N. (2016) Basic principles of ferroelectric synthesis of metal-intermetallic laminate Ti–Al$_3$Ti from foil package Al–Ti. *Electron. Obrab. Materialov*, **3**, 33–39 [in Russian].

11. Kurkin, S.E. (2016) Technology of production of layered aluminium-titanium composite material strengthened with intermetallics. *Novaya Nauka: Teoreticheskyi i Prakticheskyi Vzglyad*, **5**, 192–196 [in Russian].

12. *Hailiang* Yu, Cheng Lu, A. Kiet Tieu et al. (2016) Annealing effect on microstructure and mechanical properties of Al/Ti/Al laminate sheets. *Materials Sci. & Eng. A*, **3**, 195–204.

13. Gajanan, P. Chaudhari, Viola Acoff (2009) Cold roll bonding of multi-layered bi-metal laminate composites. *Composites. Sci. and Technology*, **0**, 1667–1675.

14. *Hailiang* Yu, A. Kiet Tieu, Cheng Lu, Charlie Kong (2014) Abnormally high residual dislocation density in pure aluminum after Al/Ti/Al laminate annealing for seven days. *Philosophical Magazine Letters,* **11**, 732–740.

15. Kaya, I., Cora, O.N., Acar, D., Koc, M. (2018) On the formability of ultrasonic additive manufactured Al–Ti laminated composites. *Metallurgical and Materials Transact. A*, **9**, 5051–5064.

16. Kaya, I., Cora, O.N., Koc, M. (2019) Formability of ultrasonically additive manufactured Ti–Al thin foil laminates. *Materials*, **2**, 1–16.

17. Sridharan, N., Wolcott, P., Dapino, M., Babua, S.S. (2016) Microstructure and texture evolution in aluminum and commercially pure titanium dissimilar welds fabricated using ultrasonic additive manufacturing. *Scripta Materialia*, **7**, 1–5.

18. Wolcott, P.J., Sridharan, N., Babu, S.S. et al. (2016) Characterisation of Al–Ti dissimilar material joints fabricated using ultrasonic additive manufacturing. *Sci. and Techn. of Welding and Joining*, **2**, 114–123.

19. Obielodan, J.O., Stucker, B.E., Martinez, E. et al. (2011) Optimization of the shear strengths of ultrasonically consolidated Ti/Al 3003 dual-material structures. *J. of Materials Proc. Technology*, **211**, 988–995.

20. *Liang* Qin, Hui Wang, Shengqiang Cui et al. (2017) Characterization and formability of titanium/aluminum laminate composites fabricated by hot pressing. *J. of Materials Eng. and Performance*, **7**, 3579–3587.

21. Krasnov, E.I., Shteinberg, A.S., Shavnev, A.A., Berezovsky, V.V. (2013) Examination of layered metallic composite materials of Ti–TiAl$_3$ system. *Aviats. Materialy i Tekhnologii*, **3**, 16–19 [in Russian].

22. *Liang* Qina, Minyu Fan, Xunzhong Guo, Jie Tao (2018) Plastic deformation behaviors of Ti–Al laminated composite fabricated by vacuum hot-pressing. *Vacuum*, **5**, 96–107.

23. *Minyu* Fan, Joseph Domblesky, Kai Jin et al. (2016) Effect of original layer thicknesses on the interface bonding and mechanical properties of TiAl laminate composites. *Materials & Design*, **5**, 535–542.

24. *Fan M.*, Luo Z., Fu Z. et al. (2018) Vacuum hot pressing and fatigue behaviors of Ti/Al laminate composites. *Vacuum*, **5**, 101–109.

25. Thiyaneshwaran, N., Sivaprasad, K., Ravisankar, B. (2018) Nucleation and growth of TiAl$_3$ intermetallic phase in diffusion bonded Ti/Al Metal Intermetallic Laminate. *Scientific Reports*, **8**, 1–8.

26. *Xu L.*, Cui Y.Y., Hao Y.L., Yang R. (2006) Growth of intermetallic layer in multi-laminated Ti/Al diffusion couples. *Materials Sc. and Eng. A*, **8**, 638–647.

27. *Shaoyuan* Lyu, Yanbo Sun, Lei Ren et al. (2017) Simultaneously achieving high tensile strength and fracture toughness of Ti/Ti–Al multilayered composites. *Intermetallics*, **0**, 16–22.

28. Lazurenko, D.V., Bataev, I.A., Mali, V.I. et al. (2016) Explosively welded multilayer Ti–Al composites: Structure and transformation during heat treatment. *Materials & Design,* **0**, 122–130.

29. Foadian, F., Soltanieh, M., Adeli, M., Etminanbakhsh, M. (2014) A study on the formation of intermetallics during the heat treatment of explosively welded Al–Ti multilayers. *Metallurgical and Materials Transact. A: Physical Metallurgy and Materials Sci.*, **5**, 1823–1832.

30. Foadian, F., Soltanieh, M., Adeli, M., Etminanbakhsh, M. (2014) The formation of TiAl3 during heat treatment in explosively welded Ti–Al multilayers. *Iranian J. of Materials Sci. and Eng.*, **11**, 12–19.

31. Fronczek, D.M., Wojewoda-Budka, J., Chulist, R. et al. (2016) Structural properties of Ti/Al clads manufactured by explosive welding and annealing. *Materials and Design*, **9**, 80–89.

IMPACT OF HIGH-FREQUENCY PEENING AND MARINE ATMOSPHERE ON THE CYCLIC LIFE OF T-WELDED JOINTS WITH SURFACE FATIGUE CRACKS

V.V. Knysh, S.O. Solovei, L.I. Nyrkova, V.G. Kot and **A.O. Grishanov**

E.O. Paton Electric Welding Institute of the NAS of Ukraine
11 Kazymyr Malevych Str., 03150, Kyiv, Ukraine. E-mail: office@paton.kiev.ua

The results of investigations of the efficiency of application of high-frequency mechanical peening technology to increase the residual life of T-welded joints of 15KhSND steel with surface fatigue cracks of 2–20 mm length and corrosion damage typical for structures after long-term service in the conditions of marine climate are presented. The long-term impact of marine atmosphere, which is typical for coastal regions of Ukraine, on the state of the surface of joints, was simulated by exposure of the samples in the salt spray chamber KST-1 for 1200 h. It was shown that surface cracks and corrosion damage significantly reduce the residual cycle life of welded joints. It was experimentally found that HFMP strengthening of T-welded joints with surface fatigue cracks of 5–7 mm length (depth is up to 1.6 mm) and characteristic corrosion damage increases their residual cyclic life to the level of welded joints with corrosion damage, strengthened by high-frequency mechanical peening at the stage of manufacturing. It is shown that in the presence of fatigue cracks of 20 mm length (about 6 mm depth), their residual life is reduced by up to 10 times, and the use of high-frequency mechanical peeening technology for such joints does not increase the cyclic life and is ineffective. 14 Ref., 2 Tables, 5 Figures.

K e y w o r d s : T-welded joints, corrosive medium, fatigue, accelerated corrosion tests, salt spray, high-frequency mechanical peening, increase in cyclic life

Technology of high-frequency mechanical peening (HFMP), also known as ultrasonic impact treatment, is widely applied to increase the fatigue resistance characteristics of welded joints of metal structures [1−6]. This technology is recommended for application to welded metal structures, operating in marine climate (bridges, overpass bridges, off-shore platforms, etc.) [7−11]. However, all the experimental data given in the above-mentioned works, were obtained under laboratory conditions in air (without corrosion impact) on samples of welded joints, which were strengthened by HFMP technology directly after welding. It is obviously believed that these structures are protected from the impact of environmental climatic factors (from corrosion) by lacquer-paint coatings. During long-term operation, however, mechanical damage, cracking and delamination of the lacquer-paint coatings can occur. This leads to the fact that the welded elements of the structures are exposed not only to alternating loading, but also to corrosive attack. In works [12, 13] the efficiency of HFMP technology application to welded structures with the specified level of accumulated fatigue and corrosion damage was studied. It is experimentally established that strengthening by HFMP technology of butt welded joints of 15KhSND

steel after prior cyclic loading ($2 \cdot 10^6$ cycles) and exposure to the impact of neutral salt spray for 1200 h (long-term impact of marine atmosphere was simulated) leads to 10 times increase of their cyclic life, and endurance limit after $2 \cdot 10^6$ cycles increases by 25 % [12]. Application of HFMP technology allows also a ten times increase of cyclic life of butt welded joints with the specified level of accumulated fatigue and corrosion damage, which are characteristic for metal structures after long-term exposure to moderate climate atmosphere of the central regions of Ukraine [13]. However, there is still no data on the effectiveness of application of HFMP technology to welded joints of metal structures, which have surface fatigue cracks of small depth, and characteristic corrosion damage, as a result of long-term service in marine climate typical for the coastal regions of Ukraine.

The objective of this work is studying the residual cyclic life of T-welded joints with surface fatigue cracks and corrosion damage, characteristic for welded metal structures after long-term service in marine climate, without and after application of HFMP technology.

Material and investigation procedure. Experimental studies were conducted on specimens of
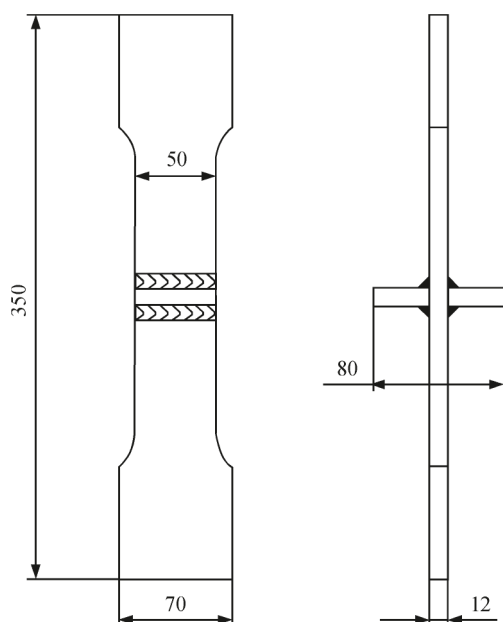
Figure 1 Shapes and geometrical dimensions of specimens of T-welded joint

T-welded joints of low-alloyed 15KhSND steel (σ_y = = 400 MPa, σ_t = 565 MPa), which is widely applied for fabrication of elements of metal structures in long-term service (for instance, in span structures of railway and road bridges), has higher strength, is readily weldable, weather-resistant and serviceable in the temperature range from minus 70 °C up to plus 45 °C.

The blanks for welded joint specimens were cut out of hot-rolled plates 12 mm thick of category 12 in the rolling direction. T-welded joints were produced by manual arc welding with electrodes of UONI 13/55 grade the transverse stiffeners (also from 15KhSND steel) to blanks of 350×70 mm size by fillet welds from both sides. The root (first weld) was made by 2 mm electrodes, the second weld was formed by 4 mm electrodes. The shape and geometrical dimensions of specimens of T-welded joints are given in Figure 1. Specimen thickness is due to wide application of 12 mm thick rolled stock in engineering welded metal structures, and 50 mm width of the working part was selected, proceeding from testing equipment capacity.

All the fatigue studies were conducted in servohydraulic testing machine URS-20 with cycle asymmetry R_σ = 0 and 5 Hz frequency at regular loading. At the first stage, fatigue testing was performed at maximum values of applied cycle loads of 180 MPa with the purpose of initiation and development of fatigue cracks of a small size on the specimen surface. This level of applied maximum loads is close to endurance limit of these joints on the base of $2 \cdot 10^6$ cycles of stress alternation [14]. To avoid complications, associated with reliable determination of fatigue crack depth, the crack reaching the specified size of 5 to

30 mm on the specimen surface was selected as the criterion of completion of fatigue testing during investigations. During these tests, the specimens in the weld zone were lubricated by indicator fluid, which consisted of kerosene and toner. After formation of a crack of specified size on the specimen surface (all the cracks formed on the line of weld metal transition to base metal), the remains of indicator fluid were removed by blowing compressed air. The indicator fluid was not used at further testing of the specimens that allowed determination of geometrical dimensions of initial cracks on welded joint fractures. After development of cracks on the specimen surface to the specified size, accelerated corrosion testing was conducted under the conditions, which simulate the impact of moderate climate atmosphere of the coastal regions of Ukraine. As the coastal regions are characterized by presence of chlorides in the environment, their long-term impact on the welded joints was simulated by specimen exposure to neutral salt spray for 1200 h, i.e. the specimens of welded joints were exposed in salt spray chamber KST-1 at the temperature of (35 ± 2) C at spraying of sodium chloride solution for 15 min every 45 min. Sodium chloride concentration in the solution was (50 ± 5) g/dm^3; pH was from 6.5 to 7.2; density was 1.03 g/cm^3. Electric conductivity of distilled water for preparation of sodium chloride solution is not more than 20 μOhm/cm at the temperature of (25 ± 2) °C. Thus, as a result of prior fatigue and accelerated corrosion testing the test specimens had damage characteristic for welded joints of metal structures after long-term service at alternating loading in moderate climate of the coastal regions of Ukraine.

When preparing for fatigue testing, the specimens with surface fatigue cracks and corrosion damage, their gripping portions were scraped again to remove corrosion damage. Scraping of the weld zone from corrosion products to metal luster was not performed. One part of the specimens was left in the unstrengthened state, and the second was strengthened by HFMP technology. Strengthening of welded joints by HFMP technology was performed by USTREAT-1.0 instrument, in which the manual compact impact tool with piezoceramic transducer is connected to ultrasonic generator with output power of 500 W. At treatment of welded joints by HFMP technology, surface plastic deformation was applied not only to the fusion line with the fatigue crack, but to all the four lines of weld metal transition to base metal of the T-joint. Single-row four-striker attachment with striker diameter of 3 mm was used as the strengthening device. Strengthening was performed without prior scraping of the surface to remove corrosion products.

Thus, fatigue testing was conducted on two series of specimens:

• specimens of T-welded joints with surface fatigue cracks 5–30 mm long and corrosion damage (first series);

• specimens of T-welded joints with surface fatigue cracks 5–30 mm long and corrosion damage, which were strengthened by HFMP technology (second series).

Experimental studies of residual fatigue life of these welded joints were performed up to complete breaking of the specimens or exceeding the test base of $2 \cdot 10^6$ cycles of stress alternation at regular loading with cycle asymmetry $R_\sigma = 0$ and 5 Hz frequency.

Test results. Description of corrosion damage which occurred in T-welded joints after corrosion testing for 1200 h in salt spray chamber KST-1 was given earlier in work [14].

Results of fatigue testing of T-welded joints of 15KhSND steel with fatigue cracks without HFMP strengthening (first series) are given in Figure 2 and Table 1. Figure 2 also shows the data on fatigue resistance of T-welded joints in the initial and HFMP strengthened states after corrosion testing for 1200 h in salt spray chamber KST-1, obtained in [14]. Table 1 gives the dimensions of surface cracks, which were determined after fatigue testing, when studying the fracture surfaces of specimens, using the indicator fluid. Fractures of T-joint specimens with surface cracks and corrosion damage are given in Figure 3. One can see that the proposed procedure allows accurately determining the geometrical dimensions of the initial crack on the fractures after specimen breaking. Despite the fact that all the fatigue cracks initiated in the fusion zone in the specimen center, the coefficient of compression of the surface crack (crack depth to half-width ratio) in them is in the range from 0.350 to 0.825. We believe that this is related to crack propa-
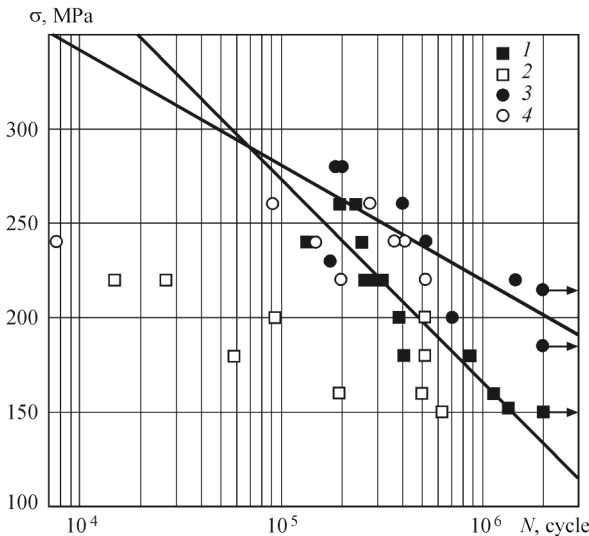

Figure 2 Experimental data of fatigue testing of T-welded joints of 15KhSND steel: *1* — in the initial state after soaking for 1200 h in KST-1 chamber [14]; *2* — after testing up to formation of surface fatigue cracks and soaking for 1200 h in KST-1 chamber; *3* — after HFMP strengthening and soaking for 1200 h in KST-1 chamber [14]; *4* — after testing up to formation of surface fatigue cracks, soaking for 1200 h in KST-1 chamber and subsequent strengthening by HFMP technology (solid lines are regression lines of data of *1* and *3*)

gation in different (by magnitude and gradient) fields of residual welding stresses, as a result of successive performance of four fillet welds by manual arc welding when manufacturing the specimens. Geometrical dimensions of the initial cracks were recorded right after specimen fracture (Table 1). However, because of rapid oxidation of the fracture surface, some of the cracks shown in Figure 3 appear to be larger than their real dimensions. All the specimens broke along the fusion line, which had an initial fatigue crack. The residual cyclic life of T-welded joints of 15KhSND steel with surface cracks of up to 1 mm depth after corrosion testing in neutral salt spray for 1200 h, is 1.5 to 2.0 times lower than the fatigue life of welded joints in as-welded state after respective corrosion

Table 1 Cyclic life of T-welded joints with corrosion damage and surface fatigue cracks

Specimen number	l_{cr}, mm	h_{cr}, mm	N_{cr}, cycles	σ_{max}, MPa	$N_{cr}^{unstrength}$, cycles	Note
2290	8	3.3	1531200	160	192900	Breaking along the fusion line
2291	5	0.9	1345200	150	630600	Same
2292	2	0.5	1950000	180	517700	»
2293	11	2.2	1136000	200	93400	»
2294	20	3.5	1353200	220	26700	»
2295	20	5.8	804800	220	14800	»
2296	5	1.0	1415300	200	516800	»
2297	15	5.8	1610900	180	58300	»
2298	9	2.1	1866400	160	500400	»

Note. l_{cr} and h_{cr} — crack length and depth before corrosion testing, respectively; N_{cr} — cyclic life up to initiation of a crack of specified length at maximum applied loads of 180 MPa; σ_{max} — maximum cycle stresses; which were applied to the specimen with a crack after corrosion testing for 1200 h in KST-1 chamber; $N_{cr}^{unstrength}$ — residual cyclic life of a specimen with a fatigue crack of the specified length and corrosion damage.
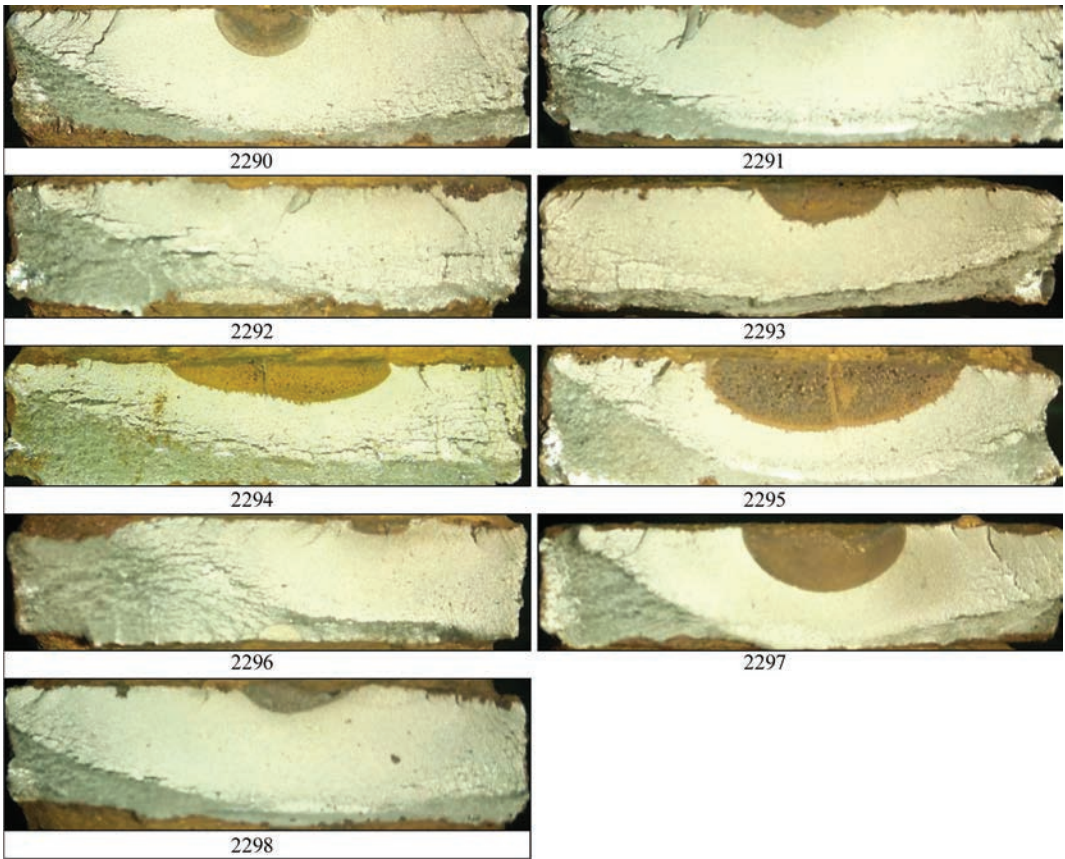
Fig re 3. Fatigue fractures of specimens of T-welded joints of 15KhSND steel with surface fatigue cracks, which were not strengthened by HFMP after corrosion testing for 1200 h in KST-1 chamber (see Table 1)

testing. With increase of the initial crack depth, the residual life of the joints becomes much lower (Table 1, Figure 2). At more than 3.5 mm depth of the fatigue crack, the residual life of the joints decreases 10 times.

Residual cyclic life of T-joints of 15KhSND steel after formation of surface fatigue cracks, soaking for 1200 h in the salt spray chamber KST-1 and subsequent HFMP is given in Table 2, and Figure 2. Table 2 also presents the dimensions of surface cracks, which

Tb le 2 Cyclic life of T-welded joints with corrosion damage and surface fatigue cracks after their strengthening by HFMP technology

Specimen number	l_{cr}, mm	h_{cr}, mm	N_{cr}, cycles	$\sigma_{cr}^{strength}$, MPa	$N_{cr}^{strength}$, cycles	Note
2197	10	3.0	826700	240	147900	Fracture along fusion line
2198	5	1.6	804100	240	407600	Same
2199	20	5.9	770400	240	7700	»
2200	5**	–	481200	260	275500	Fracture through the base metal at 55 mm distance from the weld
2201	12	2.4	760100	260	91700	Fracture along fusion line
2202	7 +3*	1.6 +0.6*	1281700	240	368200	Same
2203	5+10+5*	0.5+1.8+0.6*	452800	220	199300	»
2204	7**	–	764300	220	522800	Fracture through the base metal at 55 mm distance from the weld

Note. l_{cr} and h_{cr} – crack length and depth before corrosion testing, respectively; $N_{cr}^{strength}$ — cyclic life up to initiation of a crack of specified length; $\sigma_{cr}^{strength}$ are maximum cycle stresses, applied to a specimen with a crack after corrosion testing for 1200 h in KST-1 chamber and strengthening by HFMP technology; $N_{cr}^{strength}$ — residual cyclic life of a specimen with a crack of specified length and corrosion damage after strengthening by HFMP technology; * — specimens with several separate surface cracks along one fusion line; ** — specimens, in which crack length was established by kerosene method.
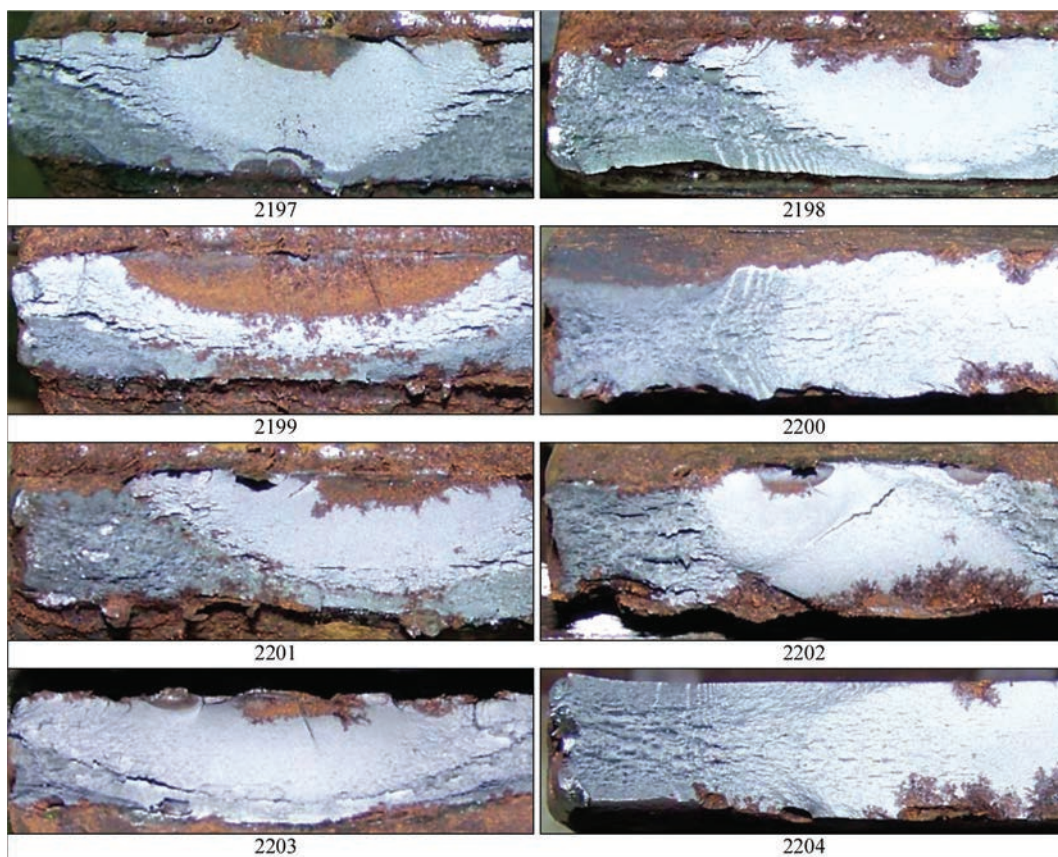
Figure 4. Fatigue fractures of specimens of T-welded joints of 15KhSND steel with surface fatigue cracks, which were strengthened by HFMP after soaking for 1200 h in KST-1 chamber (see Table 2)

were determined after fatigue testing when studying the fracture surfaces of specimens, due to application of indicator fluid. Geometrical dimensions of the initial cracks were recorded right after specimens breaking (Table 2). However, because of fast oxidation of the fracture surfaces, some cracks shown in Figure 4, appear to be larger than their real dimensions. Fracture of HFMP strengthened specimens occurred predominantly along the fusion line (Figure 5). Two specimens (No.2200 and No.2204), which had fatigue cracks 5–7 mm long (dimensions are determined by kerosene method during crack growth), after strengthening by HFMP broke through the base metal at a distance from the weld, as a result of new crack initiation from corrosion cavities in the hot-rolled surface layer of the metal (Figures 4, Figure 5). This did not allow reliable determination of the depth of the initial cracks. Considering the data of Table 1 and Table 2, however, we can state that at the moment of strengthening by HFMP, their depth did not exceed 1.6 mm. It is experimentally established that the effectiveness of application of HFMP technology, in order to increase the cyclic fatigue life, is actually determined by the geometrical dimensions of the fatigue crack before treatment. Thus, strengthening by HFMP technology of T-joints with surface fatigue cracks 5–7 mm long (of up to 1.6 mm depth) significantly increases their

cyclic life. The scatter of experimental data of such joints is within the data scatter for joints strengthened by HFMP at the manufacturing stage (without accumulation of fatigue damage) and subsequent soaking in KST chamber for 1200 h (Figure 2). After HFMP strengthening, the residual cyclic life of the joints with surface cracks of 10–12 mm length (1.8 to 3.0 mm depth) is on the level of cyclic life of unstrengthened welded joints after soaking in KST chamber for 1200 h, i.e. it is 2–3 times lower than that of HFMP strengthened joints at the manufacturing stage. Application of HFMP technology to welded joints, which

Figure 5 Specimens of T-welded joints of 15KhSND steel with surface fatigue cracks, which were strengthened by HFMP after soaking for 1200 h in KST-1 chamber, shown after fatigue testing

contain fatigue cracks of approximately 6 mm depth, is ineffective (Table 2, Figure 2).

Thus, the high effectiveness of application of HFMP technology for improvement of cyclic life was established for T-welded joints of metal structures, which have surface fatigue cracks of up to 5–7 mm length and characteristic corrosion damage, as a result of long-term service under the conditions of moderate climate of the coastal regions of Ukraine.

Conclusions

1. We performed experimental studies of the residual life of T-welded joints of 15KhSND steel with surface fatigue cracks and corrosion damage, characteristic for metal structures after long-term service in marine climate. Long-term impact of marine atmosphere, which is characteristic for the coastal regions of Ukraine, was simulated by joint exposure for 1200 h in salt spray chamber KST-1. It is confirmed that with increase of the initial crack length, the residual life of joints with corrosion damage becomes smaller. Residual cyclic life of T-welded joints with surface cracks 2–5 mm long (up to 1 mm depth) after corrosion testing in neutral salt spray for 1200 h is 1.5 to 2.0 times lower than the fatigue life of welded joints in as-welded condition after the respective corrosion testing, and residual life of joints with 20 mm fatigue cracks (more than 3.5 mm depth) decreases 10 times.

2. Studied was the application of HFMP technology to improve the residual life of T-welded joints of 15KhSND steel with surface fatigue cracks and corrosion damage, characteristic for metal structures after long-term service in moderate climate of the coastal regions of Ukraine. It was found that strengthening by HFMP technology of T-welded joints with surface fatigue cracks of up to 5–7 mm length (up to 1.6 mm depth) raises their cyclic life to the level of HFMP strengthened welded joints at the manufacturing stage. After strengthening the welded joints with surface fatigue cracks of 10 – 12 mm length (1.8 to 3.0 mm depth) their residual life is on the level of cyclic life of unstrengthened welded joints, i.e. it is 2–3 times lower than that of HFMP strengthened joints at the manufacturing stage. It is shown that application of HFMP technology to welded joints with fatigue cracks of approximately 6 mm depth does not lead to increase of their cyclic life and is inefficient.

1. Poja Shams-Hakimi, Farshid Zamiri, Mohammad Al-Emrani, Zuheir Barsoum (2018) Experimental study of transverse attachment joints with 40 and 60mm thick main plates, improved by high-frequency mechanical impact treatment (HFMI). *Engineering Structures*, **5** , 251−266.
2. Lefebvre, F., Peyrac, C., Elbel, G., et al. (2017) HFMI: Understanding the mechanisms for fatigue life improvement and repair of welded structures. *Welding in the Word*, **4**, 789−799.
3. Abbasi, A., Amini, S., Sheikhzadeh, G.A. (2018) Effect of ultrasonic peening technology on the thermal fatigue of rolling mill rolls. *The Int. J. of Advanced Manufacturing Technology*, **5−8**, 2499−2513.
4. Kudryavtsev, Y. (2018) *Rehabilitation and repair of welded elements by ultrasonic peening*: IIW Document XIII-2076−05.
5. Harati, E., Swensson, L.E., Karlsson, L., Widmark, M. (2016) Effect of high frequency mechanical impact treatment on fatigue strength of welded 1300 MPa yield strength steel. Pt1. *Int. J. of Fatigue*, 92(●), 96−106.
6. Zhang, H., Wang, D., Deng, C. (2018) Optimal preparation process for fatigue specimens treated by ultrasonic peening. *Experimental Techniques*, 42(**2**), 199−207.
7. Takanori Deluchi, Masashi Mouri, Junya Hara, et al. (2012) Fatigue strength improvement for ship structures by ultrasonic peening. *J. of Marine Sci. and Technology*, 17(**3**), 360–369.
8. Fisher, J.W., Statnikov, E., Tehini, L. .(2002) Fatigue strength improvement of bridge girders by ultrasonic impact treatment (UIT). *Welding in the World*, **9−10**, 34−40.
9. Fikri Bashar Yalchiner, Zuheir Barsoum (2017) Life extension of welded structures using HFMI techniques — potential application to offshore structures. *Procedia Structural Integrity*. **5**, 377−384.
10. Kirkhope, K.J., Bell, R., Caron, L., et al. (1999) Weld detail fatigue life improvement techniques. Pt 2: Application to ship structures. *Marine Structures*, 12(**7−8**), 477−496.
11. Martinez, L.L. (2011) Life extension of FPSO`s structural details using ultrasonic peening. *Procedia Eng.*, ● , 1059−1068.
12. Knysh, V.V., Solovei, S.O., Nyrkova, L.I, Osadchuk, S.O. (2019) The influence of marine environment on fatigue life of butt welded joints of 15KhSND steel, strengthened by high-frequency mechanical impact. *Materials Sci*. (English version in publ. within one month).
13. Knysh, V.V., Solovei, S.O., Nyrkova, L.I., Osadchuk, S.O. (2018) Influence of hardening by high-frequency mechanical impacts of butt welded joints made of 15KhSND steel on their atmospheric corrosion and fatigue fracture resistance. *Ibid*., 54 (**3**), 421−429.
14. Knysh, V.V., Solovej, S.A., Nyrkova, L.I. et al. (2016) Influence of corrosion damage on cyclic fatigue life of tee welded joints treated by high-frequency mechanical peening. *The Paton Welding J*., **9**, 42−46.

FEATURES OF SYNERGISTIC EFFECT MANIFESTATION IN LASER-PLASMA WELDING OF SUS304 STEEL, USING DISC LASER RADIATION

V.Yu. Khaskin[1], V.M. Korzhyk[1,2], A.V. Bernatskii[2], O.M. Voitenko[2], Ye.V. Illyashenko[2] and D.Cai[1]

[1]Guangdong Institute of Welding (China-Ukraine E.O. Paton Institute of Welding)
363 Chiansin Str., 510650, Guangzhou, Tianhe, China
[2]E.O. Paton Electric Welding Institute of the NAS of Ukraine
11 Kazymyr Malevych Str., 03150, Kyiv, Ukraine. E-mail: office@paton.kiev.ua

It is shown in the work that laser-plasma welding of 3 mm SUS304 stainless steel, using disc laser radiation, a stable manifestation of the synergistic effect and a ratio of powers of the laser and plasma components of 1:1–1:3 were found that allows penetration depth to be increased by approximately 25 % without any change in the welding speed. The stability of the synergistic effect and increase of penetration depth are influenced by the ratio of powers of the process components, method of feeding and composition of the shielding gas. In order to improve the hybrid welding effectiveness at coaxial feed of shielding and plasma gases, it is rational to use an additive of 2–3 % oxygen to shielding gas argon. Stabilization of the synergistic effect due to selection of mode parameters and shielding gas composition, allows replacing up to 40 % of the laser power by plasma power. The strength of joints of SUS304 stainless steel produced by hybrid laser-plasma welding is equal to approximately 95 % of that of the base metal. 8 Ref., 1 Table, 7 Figures.

Keywords: laser-plasma welding, stainless steel, synergistic effect, process experiments, penetration depth, power ratio, shielding gas

Active development of the processes of hybrid laser-arc (laser-plasma) welding of steels and alloys has been observed over the recent years [1, 2]. The interest to these processes is caused, primarily, by new technological capabilities that open up due to their application. This is related to manifestation of the synergistic effect (it is sometimes called the hybrid effect), which is manifested in violation of the additivity of thermal effect of the arc and radiation on the metal being welded, intensification of the dynamic impact of welding current on the melt pool, as well as in the change of the hydrodynamics of the pool proper. As a result, the effective efficiency of the welding process becomes higher, and the energy used for metal melting, can more than two times exceed the sum of the respective energies, evolving in the metal when using each heat source taken separately [3].

As shown by a number of studies, however, the manifestation of the synergistic effect in hybrid laser-arc processes cannot always yield the anticipated positive result, which is manifested in greater penetration depth. For instance, in work [4] it is shown that the manifestation of the synergistic effect, binding of arc plasma to the zone of laser radiation impact and process stability at high speeds, depend more on the degree of focusing of laser radiation, than on its wave length (Figure 1). In work [5] it is noted that the effectiveness of hybrid laser-TIG welding greatly depends on the kind of shielding gas and used shielding method. In work [6] it is shown that at hybrid process penetration of stainless steels, the penetration depth is influenced by the location (in the welding direction) of the component energy sources and distance between them, as well as welding current of the TIG component. Thus, studying the resultativeness of the synergistic effect and stability of its impact on increase of the penetration depth becomes urgent.

The objective of this work is determination of the possibilities for increasing the penetration depth and partial replacement of laser radiation power by plasma power, based on studying the synergistic effect manifestation in laser-plasma welding of stainless steel.

In order to determine the resultativeness of synergistic effect manifestation during hybrid laser-plasma welding, bead deposition and butt welding was performed on plates of thickness $\delta = 3.0$ mm from SUS304 steel (analog of 08KhN10) in argon atmosphere. Presence of through-thickness penetration was determined by the criterion of formation of a back bead of not less than 0.5 mm width at simulta-

V.Yu. Khaskin — http://orcid.org/0000-0003-3072-6761, V.M. Korzhyk — http://orcid.org/0000-0001-9106-8593,
A.V. Bernatskii — https://orcid.org/0000-0002-8050-5580, O.M. Voitenko — https://orcid.org/0000-0003-4946-6517,
Ye.V. Illyashenko — https://orcid.org/0000-0001-9876-0320, Д. Cai — https://orcid.org/0000-0003-2249-6097
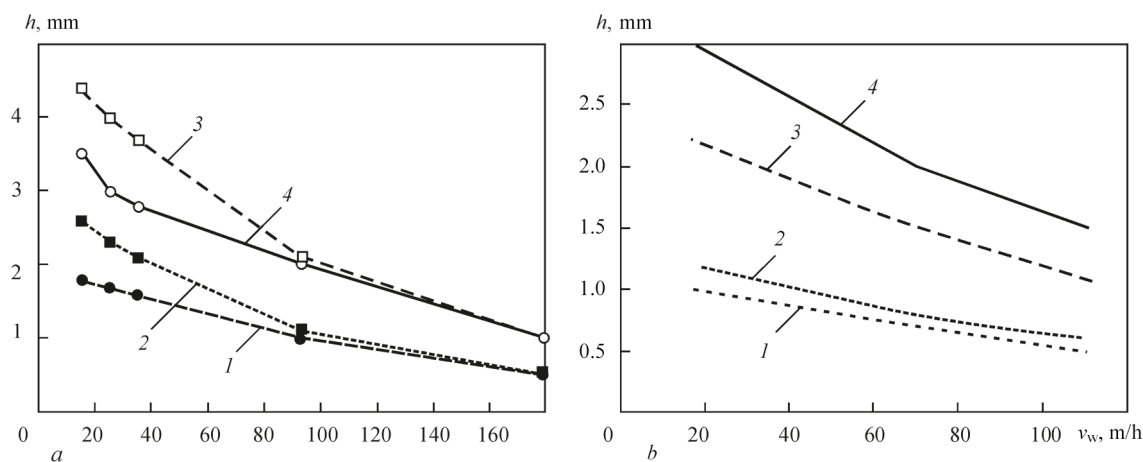
25

Figure 1 Dependencies of penetration depth *h* on speed v_w of laser-plasma welding, using diode laser radiation [4]: *a* — of 2 kW power and argon plasma of 2 kW for SUS321 stainless steel; *b* — of 1.2 kW power and argon plasma of 0.8 kW for aluminium alloy 5083 (*1* — laser welding; *2* — plasma welding; *3* — laser + plasma (arithmetic sum of *h* values); *4* — hybrid)

neous formation of quality upper bead. Undercuts and sagging of the upper bead, pores and wormholes were regarded as inadmissible defects of weld formation.

Technological studies of the process of hybrid laser-plasma welding were conducted by a scheme given in Figure 2. A disc laser with radiation wavelength $\lambda = 1.03$ μm, the power of which was changed in the range of 0.3–1.4 kW, was used during the experiments. The focal spot diameter was about 0.4 mm. Investigations were performed using an integrated co-axial plasmatron of direct action with four pin cathodes, the design of which is described in detail in [7]. The constricted arc power was up to 2.3 kW at welding current of up to 80 A. The focused laser radiation and constricted arc were taken out jointly through a

common nozzle of 2.5 mm diameter onto a welded sample located at approximately 3 mm distance from the nozzle tip. The focal plane of laser radiation was located at approximately 0.5 mm depth relative to the sample surface. Continuous-action straight polarity constricted electric arc was used in the experiments. Sheets of SUS304 steel of 200×100×3 mm size were used as samples for butt welding and bead deposition. The integrated plasmatron was moved relative to the welded sample, using an anthropomorphous robot KUKA KR30HA (Figure 3).

In connection with the impact of the kind and method of supplying the shielding gas on the obtained results, mentioned in work [5], experiment performance was started from studying the features of shielding gas supply into the weld pool formation zone. Gas was supplied through the protection nozzle made coaxial to the plasma-forming nozzle. Here, two methods were used: producing a laminar argon flow and turbulent argon flow. It was found that in hybrid laser-plasma welding the coaxial laminar supply of argon leads to a considerable (up to two times) decrease of the penetration depth and a certain increase of weld width, compared to hybrid welding using the
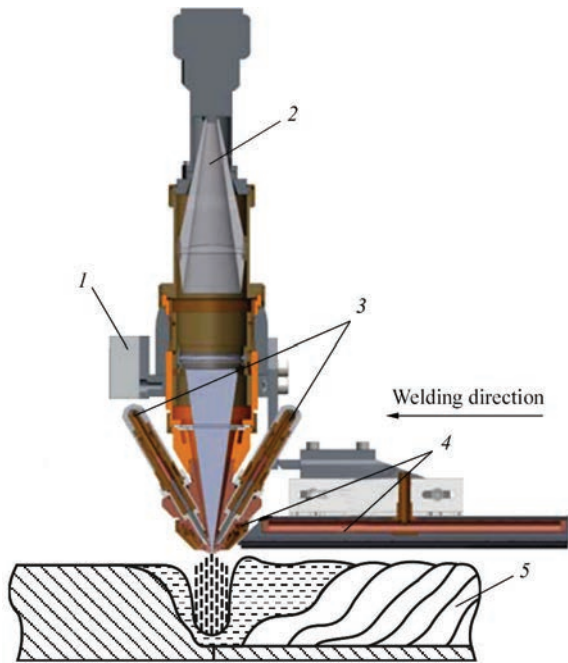

Figure 2 Scheme of experiment performance; *1* — fixing the integrated plasmatron to the robot arm; *2* — supplying laser radiation; *3* — cathode assemblies; *4* — gas shielding; *5* — sample being welded
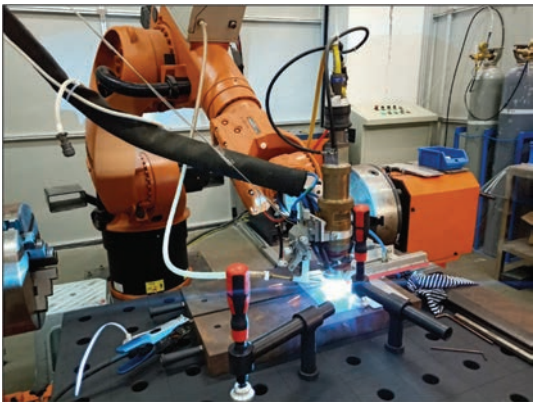

Figure 3 Appearance of the stand for laser-plasma welding with application of KUKA KR30NA robot during operation
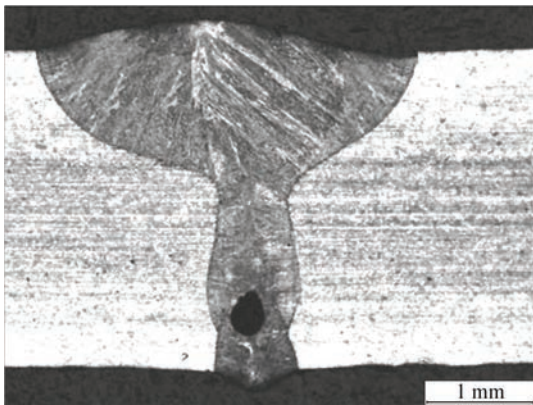
Fig re 4 Structure of the welded joint of SUS304 steel produced by laser-plasma method, with pore formation in the weld lower part

Fig re 6 Appearance of butt joint of SUS304 steel (δ = 3.0 mm): *a* — upper bead; *b* — weld root

turbulent argon supply. This is explained by penetration of a certain quantity of atmospheric air into the weld pool due to its mixing with argon, which is supplied turbulently. Let us note that an air ingress into the weld pool leads to porosity in welds (Figure 4).

It is known from study [8] that the argon-based gas composition, which includes oxygen in the amount of approximately 0.6 up to 1.9 %, allows greatly increasing the welding speed, joint tolerance and minimizing burns-through with preservation of high mechanical characteristics. No internal pores form here. Also known are the works, in which the share of oxygen in the shielding gas in welding was 3 % and higher. Therefore, in order to eliminate the negative phenomenon of pore formation at preservation of the positive
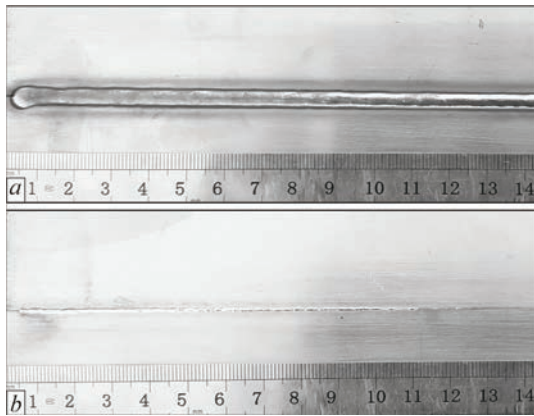
effect of increase of penetration depth, a decision was taken to use a mixture of argon with a small amount (2–3 %) of oxygen additive as the shielding gas.

After correction of shielding gas composition, and number of laser, plasma and laser-plasma bead deposits were made in different modes on a plate from SUS304 steel (Figure 5). Then butt joints were welded (Figure 6). Samples for determination of mechanical properties of the produced joints were cut out of butt joints. The nature of manifestation of the synergistic effect and its stability were established by depth and shape of the beads deposited on a plate from SUS304 steel. For this purpose transverse sections of the beads were made and their macrostructures were studied (Figure 7). Modes of bead deposition and obtained re-
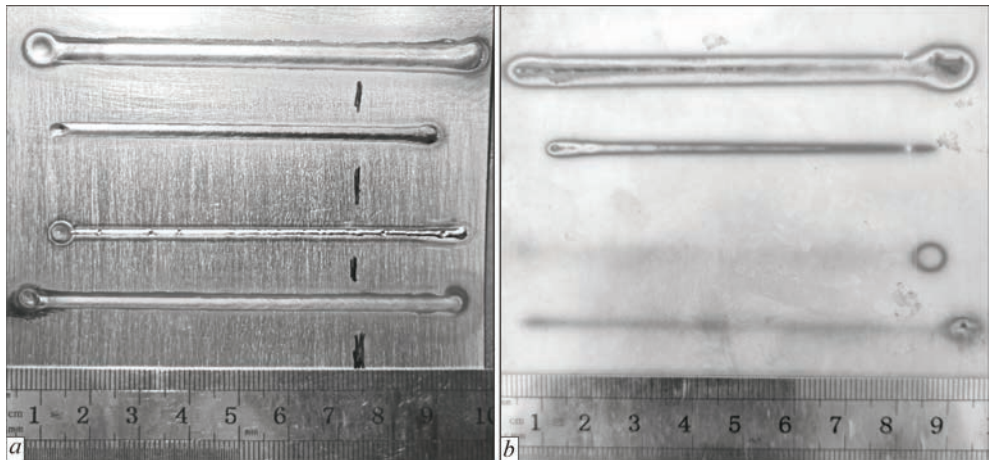

Fig re 5 Appearance of beads on a plate of SUS304 steel of thickness δ = 3.0 mm: *a* — upper side; *b* — reverse side

Welding parameters and geometrical characteristics of beads on SUS304 steel (δ = 3.0 mm) made in argon shielding at the speed of 60 m/h (1.0 m/min)

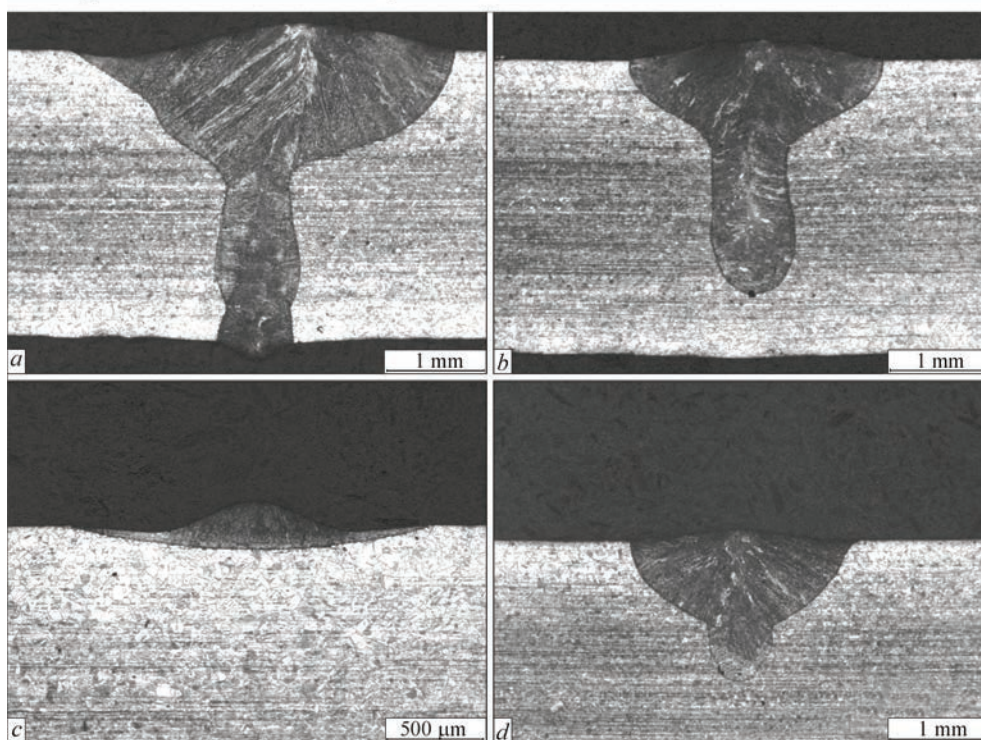| Sample number	Welding type	Radiation power, kW	Welding current, A	Width B of upper weld bead, mm	Penetration depth H, mm	Weld form factor $K = B/H$
D-1	Hybrid	1.4	80	3.94	3.46	1.2
D-2	Laser	1.4	–	2.55	2.55	1.0
D-3	Plasma	–	80	1.83	0.25	7.3
D-4	Hybrid	0.7	40	2.31	1.84	1.3

Figure 7 Macrostructure of transverse sections made in a plate of SUS304 steel of thickness δ = 3.0 mm by different methods: *a* — hybrid (sample D-1); *b* — laser (sample D-2); *c* — plasma (sample D-3); *d* — hybrid with half of the power (sample D-4)

sult (values of width *B* of the upper bead and depth *H* of penetration) are given in the Table.

During experiment performance, the high stability of manifestation of the synergistic effect in laser-plasma welding of SUS304 steel in the selected range of powers of the laser and plasma components was established, provided the ratio of these powers is kept close to 1:1.0–1:1.5. When lowering the laser radiation power from 1.4 to 0.3–0.4 kW, while simultaneously keeping the welding current on the level of 80 A (plasma component power is close to 2.3 kW), i.e. at approximately 1.6 power ratio, a reduction of penetration depth with simultaneous increase of its width was observed. The cross-sectional shape of the weld here was close to that achieved in plasma welding that leads to the conclusion of lowering of the stability of the synergistic effect manifestation.

As follows from the Table, the sum of the depth of penetrations in laser (D-2 sample) and plasma (D-3 sample) processes is equal to 2.8 mm, i.e. it is equal to approximately 20–25 % of penetration depth in hybrid laser-plasma process (D-1 sample). In the case of replacement of half (0.7 kW) of the laser power by plasma power (sample D-4) the penetration depth is equal to approximately 75 % of the depth, achieved in laser welding with total power of 1.4 kW (sample D-2). Further experiments showed that in laser-plasma welding of stainless steel, using disc laser radiation, 40 % of laser power can be replaced by plasma. Here, the ratio of laser and plasma powers in the hy-

brid process should be 1:3. Analysis of weld form factors showed that weld formation in hybrid welding is much closer to laser welding than to plasma welding (see Table).

Samples of XIII (XIIIa) type (GOST 6996–66) were cut out of joints of SUS304 steel (δ = 3.0 mm) to conduct mechanical testing. Static tensile tests were performed using a rupture testing machine of MTS Criterion 45 type on three samples with further averaging of the results. It was found that the strength of joints produced by laser-plasma method is equal to $\sigma_t \approx 750$ MPa, i.e. approximately 95 % percent of that of SUS304 base metal. Relative elongation was $\delta \approx 60$ %, i.e. 100 % relative to base metal.

The conducted studies lead to the following conclusions:

1. In laser-plasma welding of SUS304 stainless steel of thickness δ = 3.0 mm, using disc laser radiation a stable manifestation of the synergistic effect was recorded in the range of 1:1–1:3 ratios of laser and plasma components that allows increasing the penetration depth by approximately 25 % without changing the welding speed, as well as replacing up to 40 % of the laser power by plasma power.

2. The stability of the synergistic effect and increase of penetration depth are influenced by the ratio of powers of the process components and method of supplying and composition of the shielding gas. In order to improve the effectiveness of hybrid welding at coaxial supplying of shielding and plasma gases, it is

rational to use an additive of 2–3 % oxygen to shielding gas argon.

3. The strength of the produced by hybrid laser-plasma welding joints from SUS304 stainless steel is equal to approximately 95 % of base metal strength, and relative elongation is similar to this parameter of the base metal. For the majority of the welding tasks the given values are satisfactory.

1. Utsumi, A., Matsuda, J., Yoneda, M., Katsumura, M. (2002) Effect of base metal travelling direction on TIG arc behaviour. Study of high-speed surface treatment by combined use of laser and arc welding (Report 4). *Welding Int.*, 16(**7**), 530–536.
2. *Cho* Won-Ik, Na Suck-Joo (2007) A study on the process of hybrid welding using pulsed Nd:YAG laser and dip-transfer DC GMA heat sources. *J. of Welding and Joining*, 25(**6**), 71–77.
3. Seyffarth, P., Krivtsun, I.V. (2002) Laser-arc processes and their applications in welding and material treatment. London, Taylor and Francis Books. (Welding and Allied Processes).
4. Shelyagin, V.D., Krivtsun, I.V., Borisov, Yu.S. et al. (2005) Laser-arc and laser-plasma welding and coating technologies. *The Paton Welding J.*, **8**, 44–49.
5. Kah, P., Salminen, A., Martikainen, J. (2010) Laser-arc hybrid welding processes (Review). *Ibid.*, **6**, 32–40.
6. Naito, Y., Mizutani, M., Katayama, S. (2003) Observation of keyhole behavior and melt flows during laser-arc hybrid welding. In: *Proc. of Int. Cong. of Applications of Laser and Electro-Optics, ICALEO, 2003,* Jacksonville (USA). Jacksonville, LIA, Section A, 159–167.
7. Krivtsun, I.V., Korzhik, V.N., Khaskin, V.Yu. et al. (2017) *New generation unit for laser-microplasma welding.* In: *Proc. of 8th Int. Conf. on Beam Technologies in Welding and Materials Processing. Ed. by I.V. Krivtsun.* Kiev, IAW, 95–100.
8. *William* de Abreu Macedo, Vinicius de Oliveira Correia (2006) *Gas composition for arc welding. Praxair Technology, Inc., Danbury, CT (US).* Pat. US 7071438 B2: B23K9/73.

HYBRID LASER-MICROPLASMA WELDING OF STAINLESS STEEL

Welded products from thin-sheet stainless steels are made by the modern industry for the purpose of application in the fields of engineering connected with need of operation of strong enough designs, subject to corrosion and certain mechanical influences.

At the same time the task of thick welding of stainless steels up to 3.0 mm butt is often set. One of the modern innovative methods of welding, which allows to minimize residual deformations, to obtain high-quality and sound joints, is a hybrid laser-microplasma welding. In the PWI the basic technological methods of hybrid laser-microplasma welding of thin-sheet stainless steels have been developed and the choice of mode parameters has been made, as well as the mechanical and corrosion properties of the obtained joints have been studied. Hybrid laser-microplasma welding of thin-sheet stainless steels without filler wire and with its application was performed. It was determined that the use of filler wire is advisable starting with a thickness of at least 1.0 mm.

In this case, for complete melting of wire with a diameter of 0.8 mm in the case of welding with tightly joined edges, the energy inputof the process must be increased by 20–40 %, and in the case of welding with a gap between the edges by 15–30 %. The size of the gap should be about 15–20 % of the thickness of the edges. Determination of mechanical and anticorrosive properties obtained by hybrid laser-microplasma welding of stainless steel joints confirmed the prospects for industrial application of this method.

WELDING OF THERMOPLASTIC POLYMER COMPOSITES IN THE AIRCRAFT INDUSTRY (Review)

M.V. Iurzhenko[1], M.V. Korab[1], R.V. Kolisnyk[1], O.P. Masiuchok[1], A.S. Andreev[2] and V.S. Petropolsky[2]

[1] E.O. Paton Electric Welding Institute of the NAS of Ukraine
11 Kazymyr Malevych Str., 03150, Kyiv, Ukraine. E-mail: office@paton.kiev.ua
[2] Antonov Company
1 Akademika Tupoleva Str., 03062, Kyiv, Ukraine, E-mail: support@antonov.com

The volume of polymer composite structures in the aircraft industry is steadily increasing. Polymer composites based on thermosetting matrices are traditional in this field, but it is important to use new thermoplastic composites (TPCs), which have several advantages over thermosetting ones. The use of thermoplastic composite materials makes it possible to actively use welding processes in the production of structures, which significantly increases the productivity of work and reduces their cost. In the aircraft industry 3 types of heat-resistant polymers of the class of polyarylene are mostly used: polyetheretherketones (PEEK and PEKK), polyetherimide (PEI) and polyphenylene sulfide (PPS). Aeronautical structures are characterized by a large variety and complexity of forms, that's why almost all known methods of plastic welding are involved for joining. The resistance welding of polymer materials applying embedded elements made of metal mesh or carbon fabric is actively used. Induction welding technology is suitable for joining structures made of conductive carbon composites. Ultrasonic welding, laser welding, and indirect-heated tool welding are also used in aircraft engineering. Nowadays, welding processes are usually digitally controlled with permanent data storage, but currently the agenda is to move to linear process control using temperature monitoring. This paper, based on the materials of European publications, presents examples of the application of different welding methods in the manufacture of structures made of modern polymer thermoplastic composites in the aircraft industry. 16 Ref., 9 Figures.

K e y w o r d s : polymer composites, thermoplastics, welded joints, resistance welding, induction welding, ultrasonic welding

The leading aircraft manufacturer SE Antonov actively cooperates with the institutes of the National Academy of Sciences of Ukraine in order to develop and implement the advanced aircraft technologies. One of the directions of such work with the E.O. Paton Electric Welding Institute is the preparation of new polymer composite materials for the use in domestic aircrafts [1].

In modern aircraft construction, many of aircraft parts are made of polymer composites — fibrous or fabric materials impregnated with polymer matrices. The use of composites can significantly increase the weight efficiency of aerospace vehicles. In the future, their share in aircraft structures will reach 70–75 % [2]. In this field, the polymer composites are traditionally used, which are based on thermosetting matrices, however, the use of new thermoplastic composites (TPCs) is constantly growing, which have a number of advantages over thermosetting ones.

The main incentive for the use of TPC in the aircraft industry is the ability to join parts of them by welding. The welding process is a much better alternative to the traditional methods of joining parts made of thermosetting composites — mechanical mounting and adhesive bonding. Other advantages of TPC are the ability of remolding (remelting) in the process of repair and disposal, formation without complex chemical reactions and long hardening processes, no need in special storage conditions and almost unlimited storage period. This article provides a review of the main welding methods of polymer thermoplastic composites, which are used in the modern aircraft industry.

As far as aircraft elements usually operate in extreme conditions of mechanical and thermal loads, thermoplastic composites for aircrafts are made on the base of strong and heat-resistant polymer matrices. Along with traditional polycarbonates and polyamides, in this field three types of polyarylene class compounds are widely used. They include polyetheretherketones (PEEK and PEKK), polyetherimide (PEI) and polyphenylene sulfide (PPS) [3]. Polyarylenes represent carbocyclic polymers, in the molecular chains of which ring benzene nuclei are present, which represent a stable chemical structure and provide a polymer with a high thermal stability.

M.V. Iurzhenko — http://orcid.org/0000-0002-5535-731X), M.V. Korab — https://orcid.org/0000-0001-8030-1468,
R.V. Kolisnyk — https://orcid.org/0000-0002-0493-894X, O.P. Masiuchok — https://orcid.org/0000-0002-3302-3079

Polyetherketone monomers in various combinations, consist of three main components: a simple ether group, an aryl cyclic hydrocarbon group and a ketone organic compound with a double chemical bond. Depending on the number of components in the monomer, polyetherketone (PEK), polyetherketoneketone (PEKK), polyetheretherketone (PEEK) and the like are distinguished. All these polymers have a melting point higher than 330 °C and can be used as TPC matrices.

Polyetherimide (PEI) monomers also consist of three main parts: a simple ether group, an aryl ring group and an imide group derived from carboxylic acids. PEI is a high-quality fire-resistant thermoplastic matrix for TPC, which belongs to the group of heat-resistant plastics with heat resistance of up to 200 °C. It has high mechanical strength, dielectric strength, resistance to hydrolysis, ultraviolet and gamma radiation.

Polyphenylene sulfide (PPS) monomers have the simplest structure and consist of an aryl group and a sulfur atom. PPS is a relatively cheap and high-quality polymer, which is very strong, hard and dense and has a natural fire and heat resistance at the temperatures of continuous operation, being significantly higher than 200 °C. PPS is also resistant to oxidation and chemicals, it absorbs a minimum amount of water, has good electrical and excellent technical properties, as well as a low probability of deformation [4].

The vast majority of polymer structures of a modern aircraft are made of prepregs, sheet composite semi-finished products. Prepregs are produced by impregnation of the fibrous base (carbon or glass cloth of a special weaving) uniformly distributed in a layer of a polymer matrix. The leading manufacturers of modern composite materials, both thermosetting and thermoplastic, are the Companies TenCate Advanced Composites and Porcher Industries [5, 6]. Thermoplastic composite materials are available in the following forms:

● semipregs are the fabrics and unidirectional fibrous tapes, having a polymer matrix layer located only on their surface;

● prepregs of a fabric and unidirectional fibrous tapes, which are completely impregnated with a matrix polymer;

● thermoplastic laminates are a form of the material, which consists from 1 to 24 layers of reinforcing material impregnated with a thermoplastic binder. They are combined into flat sheets.

In a limited number, welded structures of TPC have been already long time used in aircraft industry and aircrafts with TPC parts have been in operation for many decades. Currently, aircraft manufacturers mostly use resistance welding and induction welding of polymer materials. Also, ultrasonic, laser and conduction welding are used [7].

The essence of resistance welding consists in the fact, that heat is produced by a flat embedded resistive element, which is located at the interface and remains inside the weld. The electric current passing through the resistive element generates heat and melts thermoplastic polymer. The working pressure on the outside of the part promotes the formation of a welded joint after switching off current and hardening the molten polymer (Figure 1). The embedded elements, usually in the form of a tape, are made of metal mesh or electrically conductive carbon fabric.

At the Berlin Air Show in 2018, Premium AEROTEC Company (Augsburg, Germany) presented a demonstration model of the bulkhead of A320 Airbus (Toulouse, France). The bulkhead consists of eight pressed segments based on TPC of carbon fiber/PPS, jointed by the method of resistance welding. On
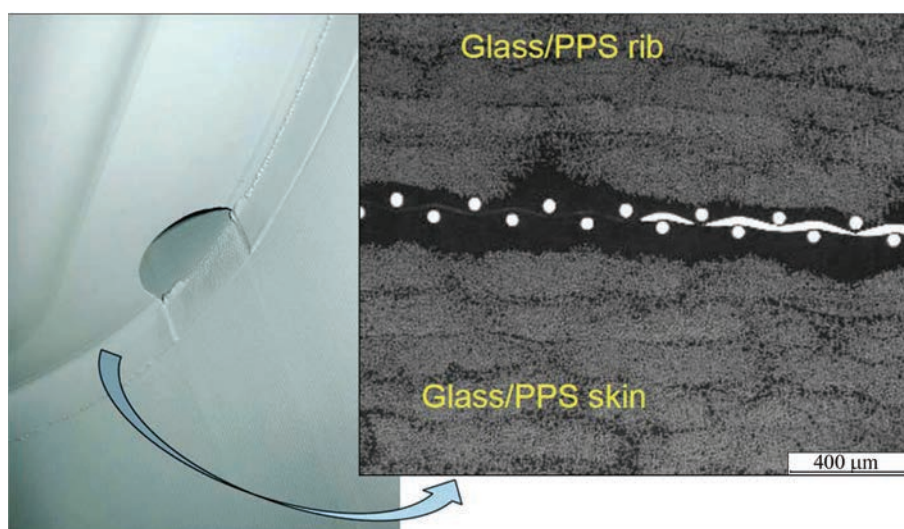

Figure 1 Resistance welded joint with metal mesh of body part and stiffener made of polyphenylene sulfide/fiberglass composite [8]
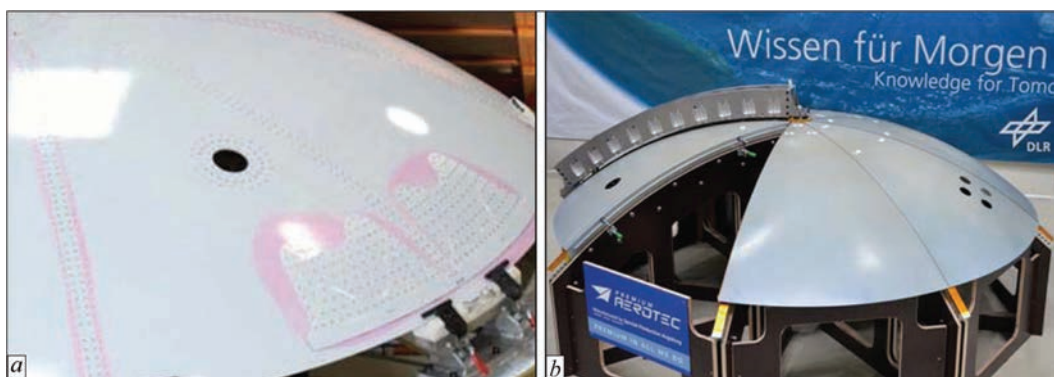
Fig re 2 Demonstration model of bulkhead of Airbus A320: *a* — acting version made of aluminum with a large number of rivets; *b* — welded demonstration model without rivets with «welding bridge»

a demonstration model of Premium AEROTEC, the length of the welds was about 1.5 m.

The thermoplastic composite bulkhead of A320 produced by welding offers the decision without rivets as compared with an existing aluminum design (Figure 2). The use of welding in this case allows saving weight, time and cost of positioning and drilling holes, as well as the cost of mounting. As embedded elements during welding, carbon fiber tapes served.

An important element of resistance welding is the working pressure, which should be applied to the parts to produce a good joint. For small parts, the working pressure is usually created by means of a robot manipulator. For large parts it is necessary to create special equipment that will provide a uniform pressure along the entire weld. In this case, the working pressure provided a bent metal «welding bridge», designed by Premium AEROTEC. By its rotation it occupies the position over each of the eight welds and creates a uniform working pressure by ten pneumatic cylinders located on it [9].

During induction welding, the coil supplied by a high-frequency alternating current, moves along the welding line and induces eddy current in the electrically conductive fibers of a carbon composite. To generate eddy current in carbon fibers, AC voltage of up to 1 MHz frequency is used. TPC based on fiberglass, which does not conduct electric current, are unfit for induction welding [10].

Using induction welding, the Company KVE Composites helped to implement the technology of production of elevating and yaw rudders for the aircrafts Gulfstream G650 and Dassault Falcon 5X [11] (Figure 3).

The Company Composite Integrity (Porquette, France) used an alternative approach and developed the technology of «dynamic induction welding», which is applied by the Company STELIA Aerospace (Toulouse, France) for joining stringers and fuselage shells based on unidirectional carbon tape and PEKK. As far as induction units, generating eddy current during welding of materials with unidirectional tapes, are absent, a special multibeam induction coil was developed. In 2016, Composite Integrity implemented the technology of induction welding to manufacture hatches for access to fuel tanks from TPC in the aircraft Airbus A220 (Figure 4).

KVE Composites showed that the use of hatches, produced by welding from TPC, allows saving costs. Even small planes can have up to 60 such access panels. Moreover, all of them have different shapes and are manufactured using a composite sandwich structure with a honeycomb core. By means of welding, all access panels can be manufactured on a one industrial site. Moreover, there is no need to perform treatment of the core. Here, the components are used, similar to the construction set LEGO: flat sheets and stamped stiffeners, which are welded with each other and form different shapes. The welding tools are relatively cheap as compared to those used today. Using welding, it is possible to manufacture all aircraft access panels of various types from TPC with the expenses on equipment, not exceeding 100 thou US dollars, which is a significant saving [11].

In 2015, the Company Composite Integrity started its work on the Project STELIA Arches TP and developed equipment for induction welding of bent parts with the size equal to that of an aircraft fuselage (Fig-

Fig re 3 Production of elevating rudders and yaw rudders by the method of induction welding from TPC carbon fiber/PPS for Dassault Falcon 5X jet aircraft

Figure 4 Fuel tank access hatches for narrow Airbus A220 aircrafts, made of TPC by the Company Aviacomp using induction welding technology developed by the Company KVE Composites

ure 5). The welding process was called «dynamic», because the robotic installation welds stringers along the length of the fuselage, the induction coil moves in three coordinates during welding, including the vertical z direction. The stringers and lining in the demonstration model of STELIA have a variable thickness. The aluminum guide serves as a clamping device and prevents the displacement of the stringer relative to the lining during welding. In the demonstration model, the working pressure was applied by means of two rollers on the welding head, which were placed above the coil. During welding, the rollers run along the stringer near the rail–clamping device, while the coil moves along the weld line. Currently, a new induction welding head was patented, which uses a single roller and improves the mechanical properties of the weld. The installation is also equipped with a device for cooling the weld, which supplies air to the surface of the joint, brings its temperature to the level lower than the crystallization limit and prevents the risk of divergence of weld elements after release of working pressure [9].

The Company GKN Fokker has gained an extensive experience in using another widespread method of welding parts from TPC: ultrasonic welding. The installation for ultrasonic welding includes electric generator of high-frequency (20–40 kHz) oscillations, piezoelectric transducer and sonotrode, which contacts with the surface of a part and provides heating and melting of a polymer matrix under the action of mechanical ultrasonic oscillations. This method was traditionally used for welding spot or small-length welds [11].

In the aircrafts Gulfstream ultrasonic welding was used to produce more than 50000 polymer parts of floor panels, manufactued from TPC by injection molding. Notwithstanding the advantages of spot welding, the ultrasonic method is very fast and highly
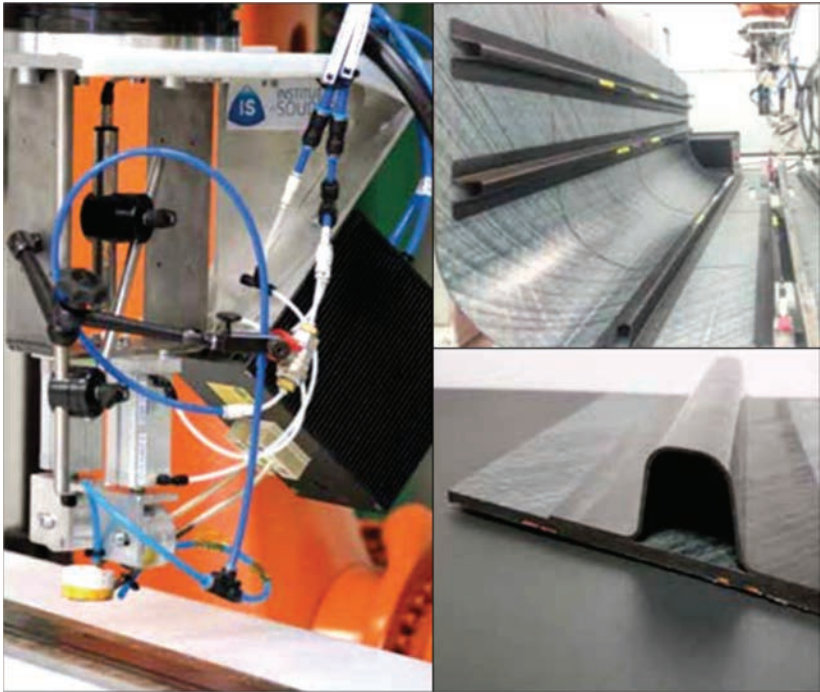

Figure 5 Induction coil and technology of welding stringers based on unidirectional carbon fiber and PEKK with lining developed by the Company Composite Integrity
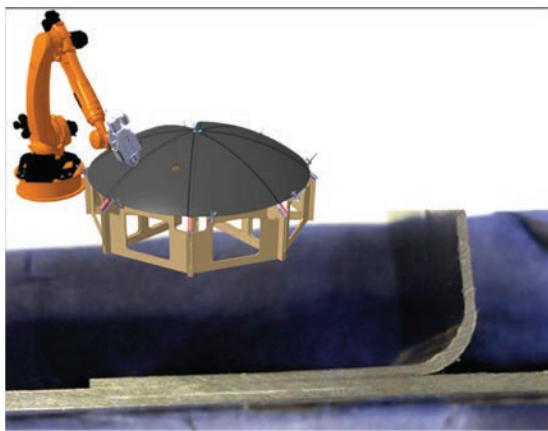
Figure 6 Ultrasonic welding head of the DLR-center and specimen of welded joint from TPC on the base of unidirectional carbon fiber and PEKK for tests on L-tear [9]

automated. The brackets of an aircraft fuselage are often joined by rivets or bolts with large structures made of thermosetting composite. Ultrasonic welding allows providing a very good joining of brackets, which are often made of nonreinforced thermoplastics.

The ultrasonic welding head of the DLR center (Augsburg, Germany) was also demonstrated, which was installed at the industrial robot KUKA and designed as an alternative to resistance welding for welding the bulkhead of the A320 aircraft from TPC (Figure 6). The mechanical tests on L-tear and comparison with the strength of mechanical joints showed promising results.

At the «31st Technical Conference, ASC» in 2016, the specialists from the TU Delft (Delft, the Netherlands) stated in their report that ultrasonic welding can be expanded to elongated welds by forming a continuous line of adjacent weld spots, which are partially overlapped. Such a continuous ultrasonic weld-
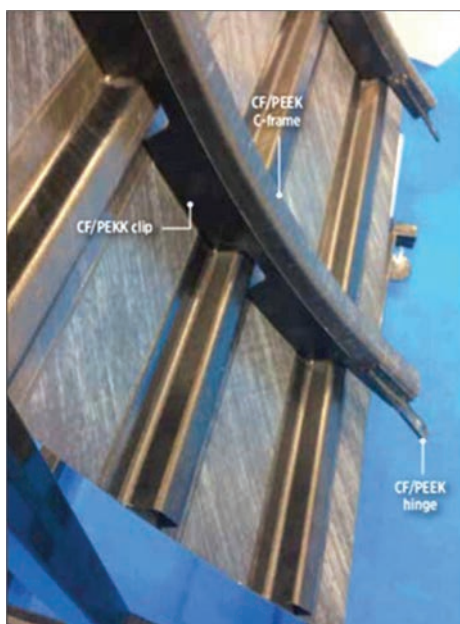

Figure 7 Sequential ultrasonic spot welding of elements made of TPC carbon fiber/PEEK

ing with producing successive points was used in the laboratory conditions to manufacture a demonstration model of the panel of the Clean Sky EcoDesign glider from TPC (Figure 7) [12].

Many cast polymer brackets of the Fokker aircraft are transparent to the laser. Therefore, there is a great potential in the use of laser welding for fixing those brackets to the fuselage structure of a carbon fiber without the need in drilling holes. The type of reinforcement and the thickness of the laminate affect the quality of the weld. However, LZH Company demonstrated good results in laser welding of PPS and PEI laminates reinforced with fiberglass.

LZH Company patented the laser technology and won the 2018 JEC World Innovation Award in the category of aerospace applications for «Modular Thermoplastic Stiffening Panels», where a stamped stiffening mesh based on thermoplastic carbon fiber is welded-on by laser to a composite shell [11].

As an alternative to induction welding, GKN Fokker Company developed a new technology for indirect heated tool welding. On the principle of «iron», the heated tool is applied to the outer surface of one of the parts and heats it through, melting the thermoplastic and partially melting the material of the lower part. The method is similar to the known method of thermal pulsed welding of polymer films. A low-inertia heater is used, due to that its heating up and cooling down takes only a few seconds. Since the entire tool is heated at once, the welding time does not depend on the length of the weld, it is the same also for the length of 0.5 and 10 m. At the exhibition JEC 2014, the fuselage panels of TPC were presented, manufactured with a heated tool. This method can work well during welding stringers of 6–10 m long with the fuselage lining (Figure 8) [11].

A key aspect for the introduction of welding technology in the manufacture of aircraft fuselage structures from TPC is the ability to monitor welding process and perform its real-time control. Nowadays, welding processes are usually digitally controlled with permanent data storage, but currently the agenda is to move to linear process control using temperature monitoring. It is supposed that the development of such technologies for resistance and induction welding requires several years, and for ultrasonic welding it may appear very quickly. Monitoring of the process of sequential spot ultrasonic welding is possible on the basis of analysis of power and shear curves, which are produced by the welding machine and allow a quick determination of the optimal welding parameters. The specialists of the aircraft industry believe that launching of welded large elements of the aircraft fuselage and possibly all welded fuselage, having no mechanical fasteners, into production will take place in the near future [11].
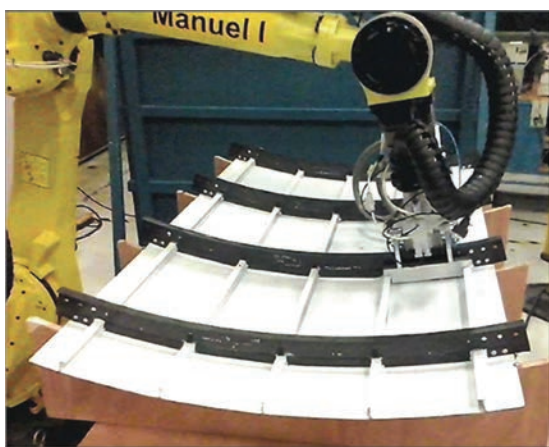
Fig re 8 Robotic head for welding elements of fuselage stringers with a heated tool using indirect heating

In the future, the introduction of additive technologies in the aircraft industry, which are currently developing in a rapid pace and introduced in the production processes of many industries, is also promising [13]. In aircraft and aerospace field, designing, development and production of complex and replaceable parts is one of the relevant issues of modern and future application of 3D printing technologies with the use of polymer materials [14], which is caused by the possibility of a significant reduction in the weight of the parts, manufactured by 3D printing, maintaining their performance characteristics [15]. Also, the parts, created by 3D printing methods are increasingly used in the manufacture of UAVs (Figure 9) [16].

Cn clusin s

A significant part of modern aircraft structures is manufactured of thermoplastic polymer composite materials based on polyetherketones, polyetherimide and polyphenylene sulfide. To join parts made of these materials, resistance, induction, ultrasonic, laser and indirect heated tool welding are used. The main areas of improvement of welding and production processes in this area are considered to be the transition to real-time process monitoring using temperature control and application of additive technologies.

Fig re 9 UAV in which 80 % of parts are printed of polymer materials

1. Kiva, D. (2012) *Aviation sector on science wings*. Viche, 21. http://veche.kiev.ua/journal/3366/ [in Ukrainian]
2. Belikov, S.B., Volchik, I.P., Mityaev, O.A. et al. (2017) *Composite materials in aircraft construction (Review)*. In: *New materials and technologies in metallurgy and machine building. 1*. http://nmt.zntu.edu.ua/article/view/131033/126779 [in Ukrainian].
3. *Chris Red* (2014) *Thermoplastics in aerospace composites outlook*, 2014-2023. Composites World, 1. https://www.compositesworld.com/articles/the-outlook-forthermoplastics-in-aerospace-composites-2014-2023
4. Callister, W.D.Jr., Rethwisch, D.G. (2015) *Fundamentals of materials science and engineering*: An Integrated Approach, Wiley; 5th Ed., 960.
5. https://www.tencatecomposites.com/resources/datasheets
6. https://www.porcher-ind.com
7. *Da* Costa, A.P., Botelho, E.C., Leali Costa, M. et al. (2012) A review of welding technologies for thermoplastic composites in aerospace applications. *J. of Aerospace Technology and Management*, **4**, 3, 255–265. http://www.jatm.com.br/papers/vol4_n3/JATMv4n3_p255-266_A_Review_of_Welding_Technologies_for_Thermoplastic_Composites_in_Aerospace_Applications.pdf
8. Offringa, A. (2016) Thermoplastic composites in aerospace. *Breakthrough Technologies for Advanced Manufacture*, Nottingham. http://www.sampe.org.uk/assets/documents/pdfs/AS2016/Presentations/AS2016_01_Arnt_Offringa_Fokker.pdf
9. Gardiner, G. (2018) Welding thermoplastic composites. *Composites World*, **9**, 50–63. ttps://sc.edu/about/centers_institutes/mcnair/documents/composites_world_september.pdf
10. Ahmed, T.J., Stavrov, D., Bersee, H.E.N., Beukers, A. (2006) Induction welding of thermoplastic composites — an overview. *Composites,* Pt A, 37(❶), 1638–1651. https://www.deepdyve.com/lp/elsevier/induction-welding-ofthermoplastic-composites-an-overview-ps031YzeOD
11. Gardiner, G. (2008) *New horizons in welding thermoplastic composites* https://www.compositesworld.com/blog/post/new-horizons-in-welding-thermoplastic-composites
12. Palardy, G., Villegas, I.F. (2016) Smart ultrasonic welding of thermoplastic composites. In: *Proc. of the Conf. on American Society for Composites — 31st Techn., ASC*. https://pure.tudelft.nl/portal/fi les/12482685/1816.pdf
13. *Aerospace 3D Printing Market Size, Share & Industry Analysis, By Vertical (Printers and Materials)*, By Industry Type (UAV, Aircraft, and Spacecraft), *By Application Type (Engine Components, Space Components, and Structural Components), By Printer Technology Type* (DMLS, FDM, CLIP, SLA, SLS and Others), and Regional Forecast 2019–2026. https://www.fortunebusinessinsights.com/industryreports/aerospace-3d-printing-market-101613
14. Joshi, Sunil & Sheikh, Abdullah. (2015). *3D printing in aerospace and its long-term sustainability. Virtual and Physical Prototyping*. ❶ , 1–11. 10.1080/17452759.2015.1111519. https://www.tandfonline.com/doi/abs/10.1080/17452759.2015.1111519?journalCode=nvpp20
15. *3D printing in aviation — advantages and areas of application* https://www.mototok.com/blog/3d-printing-in-aviation-advantages
16. *TOP 10 3D Printing in Aeronautics* https://www.3dnatives.com/en/3d-printing-aeronautics-010320184/

ABOUT THE OLDEST TECHNOLOGY OF BRAZING ON THE EXAMPLE OF ARCHAEOLOGICAL FINDINGS — A GOLDEN GOBLET FROM TRIALETI AND A MUFFLE FROM KVATSKHELI

Er.M g d ze

National Museum

3 Furtseladze Str., 0105, Tbilisi, Georgia. E-mail: e.magradze@gmail.com

Considering the stages of human development from a material and spiritual point of view, a significant achievement in this field is the discovery and study of metals, as well as the invention of methods for their processing. The result of activity and constant search in this direction is the creation and development of metallurgy. The masterpieces of jewellery are presented to us as a continuation of these processes. An integral part of these processes is the accumulation of knowledge through observation and improvement of the learned rules and techniques. One of the most important of them is the brazing process as a method of joining finished metal parts that was invented by a human at an early stage of human development. 8 Ref., 8 Figures.

K e y w o r d s : brazing, reaction and substance brazing alloy, metallic gold, brazing of artifacts

The aim of this study is to present the tools and technologies existing in ancient jewellery workshops and also to make the conclusions about the composition of the brazing alloy and the methods of its application based on the results of the works on joining parts using brazing.

Based on the made observations, I can say that on the oldest products, traces of two types of brazing alloy are observed. The first is «substance brazing alloy», during which to a gold or silver product a melt of a small amount of gold or silver (from the same metal that the product is made of) is applied, with the addition of a special alloying metal.

And the second, the so-called reaction brazing alloy, which contains a complex chemical compound of organic and inorganic substances. Under the influence of temperature, as a result of reducing reaction, this compound melts the surface of the products and firmly joins the smallest parts between each other.

Today, at modern jewellery workshops, during brazing of silver or gold products, only the first method is used. That is, to achieve the desired results and the required temperature, «substance brazing alloys» are used. For their manufacture, gold or silver is taken, however their amount should be small and with the addition of alloying metals. The latter include elemental silver, copper, lead, zinc, tin, cadmium, etc. By introducing these metals into the basic composition of gold or silver in various proportions, special alloys are produced, that strongly join two parts of the product with the use of appropriate fluxes and temperature [1].

During brazing, gas torches are used, among which there are many types; we can use them based on the specified task. They are quite easy in using and allow the craftsman to make an efficient processing of the details. These appliances easily regulate the flame with the help of a special valve, increasing or decreasing the gas flow [1].

In the process of changing the cultural epochs of human development, jewellery began to flourish and the primary metal gold, necessary for such a work was considered to be sacred, it was considered to belong to the gods [2].

The works of many authors of the Middle Ages, which have survived to this day, tell us both about the metal processing in general as well as about jewellery: Al Birun, Theophilus, Arraz, Agricola, Beringuchio, Cellini, Vakhtang VI, etc.

Considering the history of processing precious metals, a researcher cannot ignore one of the most important manuscripts belonging to the pen of Theophilus Presbyter, Benedictine monk, who worked in the XI–XII centuries [3].

For our study, the treatise of Theophilus was particularly interesting as far as it discusses the methods for preparing the gold base for cloisonne enamel and the manufacture of partitions for enamel. It also provides some advice on the preparation of brazing alloy and its application [3].

Theophilus considers two types of brazing alloy:
● produced by alloying gold or silver;
● manufactured from chemicals.

The second type of brazing alloy, as indicated above, is prepared from such organic and inorganic compounds, which melt the surface of gold or silver at a temperature of 900–920 °C and join two parts between each other. Such a method originated in the distant past of mankind, and the advanced nations of the ancient world used that method to create exquisite art forms such as filigrain and granulation based on the processing of such natural materials as chrysocolla (aqueous copper silicate $CuSiO_3$ nH_2O) or malachite (aqueous copper carbonate $Cu_2[CO_3](OH)_2$). According to Theophilus, the composition of the brazing alloy is valuable because it describes a method for producing this brazing alloy using artificial chemical processes in the developed Middle Ages [3].

In his treatise the methods of brazing jewellery are described by the Italian jeweler and sculptor of the XV century Benvenuto Cellini. He describes the contents of alloying (substance) brazing. As far as defects are almost always formed during calking in the form of holes and cracks, it is necessary to fill them with this type of brazing alloy [4].

He proposes to eliminate the mentioned defects only with the help of substance brazing, since reaction brazing is not able to eliminate the errors because of the lack of substance. The latter allows melting the surface of the precious metal, which is a good method for joining each small part.

P. Theophilus also indicates the need in preparation of alloying and substance brazing. However, unlike Cellini, instead of silver he introduces copper into gold [3].

The king Vakhtang VI, a Georgian scientist of the 17th–18th centuries, also writes about alloying gold with copper in his treatise «Book about the preparation of solutions and chemical transformations» [5].

These examples clearly indicate the existence of universal uninterrupted knowledge in the field of processing precious metals. And although they were always strictly hidden, nevertheless they spread and adopted the characteristic features of one common culture of mankind.

After describing the application and content of the brazing alloy, Theophilus writes about the way a craftsman should do his brazing work. He points out on how a space in a bunch of burning coal can be created so that the product does not directly come in contact with fire, and a certain temperature would uniformly surround the parts to be joined. That is, as also Cellini later did, he is trying to create a muffle-like space in a bunch of burning coals. Although Theophilus is familiar with the method for manufacturing iron muffle for calcination of enamel and he even describes that method [3], he still offers another

Artifact, muffle «Colchian cover»

method for brazing, apparently in order to be able to follow the process. And the iron muffle necessary for calcination of enameled plates is described by him as follows: «Put the plate into fire on a thin sunken tray with a short metal handle. Cover it with an iron lid, which should be concave like a small bowl and also completely covered with holes ... This lid should also have a small ring in the middle, by means of which one could cover and open it ... ».

The small appliance made of iron, described by Theophilus, which apparently was used in the Middle Ages, consists of two independent parts: a lower concave tray with a handle and a round hemispherical iron lid with a ring. Combining of these two parts creates an enclosed space — a muffle. The name «muffle» comes from the Latin word muffla, in French moufle, which means «coupling» or «closed».

It is interesting to know whether such a appliance existed in earlier times, and what modifications could exist or what materials had to be used.

In 2012–2013 in the National Museum of Georgia I realized the project «On the Traces of Lost Technologies — Cloisonne Enamel», within the framework of which it was planned to investigate the peculiarity of technologies of a Georgian-Byzantine cloisonne enamel. In the process of the work on the project, I was able to identify an artifact from the Vani fortification, a cone-shaped product made of sheet iron with many holes, dating back to the middle of the 1st

Copy of the muffle «Colchian cover»

millennium BC. This appliance consists of two parts made of hammered iron. The same as in the muffle described by P. Theophilus, it has a lower concave part and a tightly closed conical-shaped lid with a metal ring at the top.

After studying and reconstructing the so-called Theophilus lid, it became easier to identify the lid from Vani. That was definitely a muffle. As soon as we put this appliance into fire, a high temperature is formed inside the chamber and, as experiments showed, that provides us the ability to glaze small ceramic products, calcinate the enameled plate, and also join (braze between each other) the finest parts of gold and silver. The reconstruction of the described product and many experiments showed that it meets the requirements for all of the abovementioned jewellery operations.

From all the mentioned above it was concluded that P. Theophilus, creating his treatise, knew and used the traditional knowledge of the jewellery workshop of the ancient world. The artifact from Vani was called a «Colchis cap» by us [6].

Naturally, the question arises whether such an appliance should have been known in earlier times and that in the design of the Colchis cap the usefulness and wisdom of the knowledge of the ancient craftsmen is seen.

Over the long years of work in this area, my attention was drawn to two products of refractory clay covered with holes, which are stored in the National Museum.

One of those two artifacts was discovered during archaeological excavations in the Kartlii district near the village of Urbnisi on the Mountain Tvlepiya [7] and the second one in the Southeast Georgia in the Dedoplists-karo region. They date back to IV–III thous BC. One of those two lids, found in the village of Urbnisi, has a lower part that fits perfectly with the mentioned clay lid and was found by archaeologists in 1956.

In 2018, at the National Museum of Georgia, we realized a scientific project called «Wisdom embodied in gold — a golden goblet from Trialeti». Within the framework of the project, I had to study the technology of creating a historical cultural monument, which was decorated with applied ornaments and various decors of the golden goblet, found in the Southeast Georgia on the Trialeti Range, the famous center of the kurgan culture in the 1930s and refers to the beginning of the II millennium BC.

Technologically, this goblet is the object of a very complex design. There is no such kind of jewellery, applied even in later eras, which would not have been used in this goblet. It is decorated with carnelian, azure, agate, amber and finely processed minerals. And such the most beautiful product decorated with filigrain and granulation, cloisonne forms are brazed-in filled with a coloured jewellery paste. It was found that this goblet was made by local jewelers and represents an example of the finest art that has no analogue [8].

First of all, during the investigation, I was interested in how many brazing methods were used by the craftsman to create this goblet. After examinations under a microscope, it became clear that the gold sheet plates were brazed-in using an alloyed or substance method. This is confirmed by the fact that in some places unmelted rectangular fragments of brazing alloy were preserved.

This indicates that some brazing alloy plates were prepared in an alloyed manner that did not melt during the first heating, and the craftsman was careful

Artifact, «golden goblet from Trialeti»

Unmelted fragments of substance brazing alloy
on the artifact golden goblet from Trialeti

not to heat the product for the second time. Just because of the fact that in some places the details of the product were not thoroughly brazed, during the burials throughout the centuries, the goblet was deformed and as a result, the applied ornaments were partially torn off from its body.

A detailed examination reveals that the craftsman also applied another type of brazing alloy. In particular, the applications on the goblet itself, filigrain on the leg, frames for stones and granulation are clearly brazed by the method that was used in the subsequent centuries to join partitions, filigrain and granulation. That was the method described by P. Theophilus and later by Cellini. Applying this brazing alloy on the surface of the product, traces of light erosion are revealed.

This type of brazing alloy acts on the surface of the metal without penetrating inside [5]. The indicated method of brazing precious metals for joining balls of granulation, golden partitions and the finest filigrain, was used by the nations of ancient civilizations. According to observations, to join the larger parts, alloyed or substance brazing alloys were used. This was once again confirmed by a detailed study of the chemical composition of the Trialeti goblet using a portable nondestructive X-ray fluorescence analyzer. The four parts of the goblet were studied that are interesting to us. Here are the results of this study:

Edge . . . . Au–83.4; Ag–11.9; Cu–3.6; Fe–0.291; Middle
outside part of the goblet Au–83.1; Ag–12.9; Cu–3.59; Fe–0.348;
Filigrain Au–82.8; Ag–11.7; Cu–4.55; Fe–0.283;
Leg of the goblet . . . . Au–80.1; Ag–15.7; Cu–3.31.

These scientific observations confirm the many-year studies in this area. In particular, at the places of joint, an excess of alloyed metal is observed unlike in the main area. In the place where filigrain is located, a slight increase in copper content is observed. That is correct, as far as when a brazing alloy of the reaction type is used, the principle of the reduction of copper from the oxide state to the state of the metal works. As a result, the thinnest copper film is formed on the surface of gold, which under the influence of high temperature is strongly joined with gold and forms a layer having a low melting point. This phenomenon occurs as fast as a flash and very carefully joins small parts between each other.

The conducted chemical analyses on the composition of the goblet show an increase in silver content in the places where substance brazing alloy had to be applied. We can make a bold assumption that this brazing alloy is made of gold with the addition of silver and copper, where silver prevails.
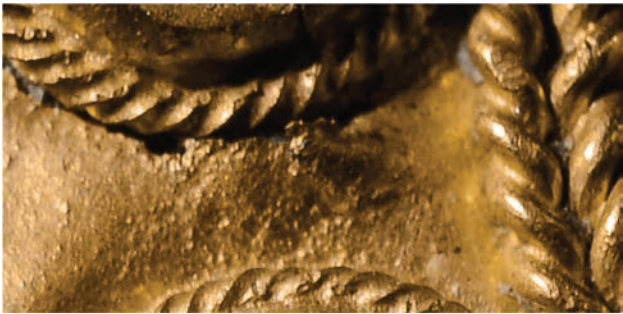
Traces of reaction brazing alloy
on the artifact golden goblet from Trialeti

I think that the results of the study of the Goblet from Trialeti are of great importance in the field of technologies for studying artifacts and brazing.

All of the abovementioned is confirmed by the recipes of the brazing alloy and the methods of their application described by P. Theophilus and B. Cellini. Both authors emphasize that for a reliable joining of large parts, a craftsman should use metal or substance brazing. The authors of the treatise apply it in a sawn state [4].

The fragments of unmelted brazing alloy and erosion around the inlaid and granulation-covered part of gold found on the golden goblet from Trialeti, make it clear that in that region already at the beginning of the II millennium BC both types of brazing alloy and methods for their application were known.

Conducting the investigations with the Trialeti goblet, I tried to find out what kind of tools were indeed used by the creator of this masterpiece. As far as in the jewellery a great importance is paid to joining parts, in the course of the project we reconstructed the ancient instruments of labour and tools used during such ling of work. As was confirmed during the experiment with the «Colchian cover», it turned out to be a jewellery appliance for calcination of products. We conducted the same experiments with the muffle from Kvatskheli, which is entirely made of clay and is very similar to the «Colchian cover». We were interested whether an ancient craftsman could use that appliance to perform operations requiring a high and stable temperature.

According to its design, the Kvatskheli muffle consists of two parts, the lower one is the chamber for fire and the upper one adjacent to it, is the lid reflecting heat. In turn, the lower part, intended for fire, fits tightly to the hollow sphere with its edge, the same sphere stands on three legs joined by a common bottom. Below, this sphere-shaped bowl has a hole for air supplied into the chamber. Inside the combustion chamber, a very high temperature is formed, heating air in the lower part. Due to a strong fire, the bottom of the chamber is incandescent and it heats up air in the sphere. A jet of hot air is mixed with cold air enter-

Ceramic muffle from Kvatskheli

ing from the lower sphere and is supplied warm into the chamber with burning coals. It is known that with the help of warm air the fuel heats up twice as fast and burns more economically and stably accumulates heat under the reflective lid. This creates excellent working conditions.

We created a muffle furnace from clay similar to that from Kvatskheli and made a lot of experiments with it.

In the chamber for fire under the reflective lid, heat is formed and maintained and the temperature is more stable and uniform there than in modern torches for brazing, which do not allow creating the fire that grows in its intensity, necessary for brazing parts. Whereas in the muffle, created on the example of the Kvatskheli artifact, the manufactured product is heated easily, and the most important is that heat is spread uniformly over the entire surface. This is a prerequisite for high-quality successful brazing.

With the help of theoretical studies and numerous practical experiments, we proved that with the use of the Kvatskheli type muffle, many jewellery operations such as melting gold or silver in small crucibles, calcinating of the hammered parts and their joining using brazing can be carried out. This muffle represents a laboratory appliance of a complex design, which was used by ancient craftsmen-jewellers in their workshops already at the end of the 4th and beginning of the 3rd millennium BC.

The appliances of a similar type dating back to later centuries are also found by us during excavations. A striking example here is an iron muffle with windows found during excavations in the Vani fortification (Western Georgia), which was named the «Colchian cover» by us. And later on, P. Theophilus writes about the lid for calcinating enamel in his treatise.

Thus, the types of brazing carefully studied by us on the example of the Trialeti goblet and the ex-
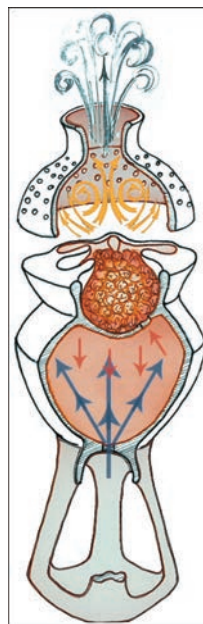
Principal scheme of functioning of «ceramic muffle» from Kvatskheli

periments carried out with the Kvatsheli muffle give ground to suggest that almost at the entire territory of modern Georgia, there were craftsmen of the highest class, who perfectly mastered the technology of processing non-ferrous and precious metals. The artifact, dating back to the beginning of the 2nd millennium BC, found by archaeologists on the Trialeti ridge, evidences that there was a whole system of jewellery workshops based on deep knowledge. And our artifact, a golden goblet from Trialeti is a worthy confirmation to that.

1. Brepol, E. (1982) *Theory and practice of jewellery making.* Leningrad, Machinostroenie [in Russian].
2. Khaushka, R. (2004) *Theory about substance*. Kaluga, Dukhovnoe Poznanie [in Russian].
3. Theophilus. (1979) *On divers arts*. New York: Djver Publ. Inc.
4. Vahtang, V.I. (Bagrationi) (1981) *Book on preparation of solutions and chemical transformations*. Tbilisi, Tb. Un-t [in Georgian].
5. Cellini, Be (2003) *Biography. Treatises. Poetry*. St.-Petersburg, Azbuka [in Russian].
6. Magradze, E. (2014) Manifesting of the early antique goldsmith workshop in site of ancient Vani on the example of Colchian Cover. *Bull. of the Georgian National Museum. Series of Social Sci*. Tbilisi, 50B, 323–340.
7. Dzhavakhishvili, Al., Glonti, L. (1962) A*rcheological excavations performed during 1954–1961 in Kvatskhelebi village (Tvlepia-Kokhu)*. Urbnisi, Tbilisi. Academy of Sci. of Georgian SSR [in Georgian].
8. Kuftin, B.A. (1941) *Archeological excavations in Trialeti. Ibid.*